blood®
Regular Article

MYELOID NEOPLASIA

BMP2/SMAD pathway activation in JAK2/p53-mutant megakaryocyte/erythroid progenitors promotes leukemic transformation

Bing Li,[1,2,*] Wenbin An,[1,2,*] Hua Wang,[3,4,*] Timour Baslan,[5] Shoron Mowla,[1] Aishwarya Krishnan,[1] Wenbin Xiao,[1,6] Richard P. Koche,[4] Ying Liu,[1,6] Sheng F. Cai,[1,7] Zhijian Xiao,[2] Andriy Derkach,[8] Ilaria Iacobucci,[9] Charles G. Mullighan,[9] Kristian Helin,[3,4] Scott W. Lowe,[5,10] Ross L. Levine,[1,7,11] and Raajit K. Rampal[1,7]

[1]Human Oncology and Pathogenesis Program, Memorial Sloan Kettering Cancer Center, New York, NY; [2]State Key Laboratory of Experimental Hematology, National Clinical Research Center for Blood Diseases, Institute of Hematology & Blood Diseases Hospital, Chinese Academy of Medical Sciences & Peking Union Medical College, Tianjin, China; [3]Cell Biology Program, [4]Center for Epigenetics Research, [5]Cancer Biology and Genetics Program, [6]Hematopathology Service, Department of Pathology and Laboratory Medicine, [7]Leukemia Service, Department of Medicine, and [8]Department of Epidemiology and Biostatistics, Memorial Sloan Kettering Cancer Center, New York, NY; [9]Department of Pathology, St. Jude Children's Research Hospital, Memphis, TN; [10]Howard Hughes Medical Institute, New York, NY; and [11]Center for Hematologic Malignancies, Memorial Sloan Kettering Cancer Center, New York, NY

KEY POINTS

- **Aberrant activation of the bone morphogenetic protein/SMAD pathway is a key mediator of p53 mutant LT of MPNs.**
- **Genomic instability and DNA damage characterize p53 mutant LT of MPNs, rendering this leukemia sensitive to DNA damage repair inhibitors.**

Leukemic transformation (LT) of myeloproliferative neoplasm (MPN) has a dismal prognosis and is largely fatal. Mutational inactivation of *TP53* is the most common somatic event in LT; however, the mechanisms by which *TP53* mutations promote LT remain unresolved. Using an allelic series of mouse models of *Jak2/Trp53* mutant MPN, we identify that only biallelic inactivation of *Trp53* results in LT (to a pure erythroleukemia [PEL]). This PEL arises from the megakaryocyte-erythroid progenitor population. Importantly, the bone morphogenetic protein 2/SMAD pathway is aberrantly activated during LT and results in abnormal self-renewal of megakaryocyte-erythroid progenitors. Finally, we identify that *Jak2/Trp53* mutant PEL is characterized by recurrent copy number alterations and DNA damage. Using a synthetic lethality strategy, by targeting active DNA repair pathways, we show that this PEL is highly sensitive to combination WEE1 and poly(ADP-ribose) polymerase inhibition. These observations yield new mechanistic insights into the process of p53 mutant LT and offer new, clinically translatable therapeutic approaches.

Introduction

BCR-ABL–negative myeloproliferative neoplasms (MPNs) are characterized by somatic mutations (eg, *JAK2*, *CALR*, and *MPL* mutations) that activate the JAK-STAT pathway.[1-4] In a substantial proportion of cases, MPNs undergo leukemic transformation (LT), which carries a dismal prognosis and often does not respond to classical antileukemic therapies.[5,6] The most frequent genomic alterations to occur at the time of LT involve *TP53* (mutated in approximately one-third of patients at time of LT[7,8]), in marked contrast to the low frequency of *TP53* alterations in the chronic phase of MPN (2%-5%).[8,9] In addition, alterations in chromosome 17p, which contains the *TP53* locus, predict a high likelihood of LT and are commonly observed in LT.[10,11] These data thus indicate that *TP53* alterations are a key regulator of the process of LT.

We have previously shown that the variant allele fractions of *TP53* mutations are significantly greater in post-MPN acute myeloid leukemia (AML) than in MPN. In the majority of cases, the *TP53* mutated clone had a variant allele fraction >50% at the time of LT, consistent with selection for biallelic *TP53* inactivation. By contrast, previous studies have shown that low abundance *TP53* mutations do not necessarily influence disease progression in MPNs and that *TP53* haploinsufficiency may be insufficient for blast phase transformation.[12,13]

The vast majority of patients with myeloid malignancy carry *TP53* missense mutations, most of which are located in the DNA-binding domain.[8,14,15] However, the mechanisms by which *TP53* mutational status, as well as allelic configuration, drives disease progression remains largely unknown. We have previously shown that in a *Trp53* knockout background, overexpressed *JAK2*^{V617F} promotes LT, consistent with observations in humans.[7] Here we seek to investigate the impact of *Trp53* mutation status as well as allelic state on the process of LT and to identify the mechanisms of LT mediated by alteration of *Trp53*.

Materials and methods

Mice

Jak2^{V617F} knock-in mice[16] were crossed to *Rosa-Cre*ERT2 and *Trp53*^{R172H} knock-in[17] and *Trp53* knock-out[18] mice. Cre expression was induced by oral gavage of tamoxifen one time at a 4-mg dose. Deletion/recombination was confirmed 2 weeks after tamoxifen oral gavage. Murine transplant procedures are described in the supplemental Methods (available on the *Blood* Web site). Mouse husbandry, care, and all animal interventions were in strict compliance with the Institutional Animal Care and Use Committee guidelines.

Flow cytometry and fluorescence-activated cell sorting

Antibody staining for surface marker was performed as previously described.[19] The antibodies used are listed in the supplemental Methods.

In vitro colony-forming assays

Cytokine-supplemented methylcellulose medium (STEMCELL Technologies, M3434) was used for colony-forming assays as previously described.[20]

RNA-sequencing

For RNA-sequencing (RNA-seq), RNA was isolated by TRIzol extraction from sorted-cell populations as indicated. RNA-seq libraries were generated by 3′ sequencing and SMART-Seq2 amplification and sequenced on an Illumina HiSeq 4000.

Single-cell RNA-seq

Lin$^-$c-Kit$^+$ bone marrow (BM) cells from mice were sorted for viability (4′,6-diamidino-2-phenylindole negative). Single-cell RNA-seq (scRNA-seq) libraries were prepared following 10X Genomics protocols (Chromium Single Cell 3′ Reagent Kit version 3). The final libraries were assessed by using an Agilent Technology 2100 Bioanalyzer and were sequenced on an Illumina NovaSeq 6000 system (S2 flow cell, paired-end).

Western blot

Western blot was performed as previously described.[20] The antibodies used are listed in the supplemental Methods.

Results

Loss or mutation of *Trp53* synergizes with *Jak2*^{V617F} to induce a highly penetrant erythroid leukemia

To investigate the genetic interactions between *Trp53* deficiency and recurrent *Trp53* mutations and *Jak2*^{V617F} signaling in leukemogenesis, we generated an allelic series of genetically engineered mouse models (supplemental Figure 1A). To investigate the cell autonomous interaction between *Trp53* loss or mutant *Trp53* and *Jak2*^{V617F}, we transplanted BM cells from wild type (WT), *Jak2*$^{V617F/+}$ (J^{VF}), *Jak2*$^{V617F/+}$ *Trp53*$^{+/-}$ (J^{VF}P$^{+/-}$), *Jak2*$^{V617F/+}$ *Trp53*$^{-/-}$ (J^{VF}P$^{-/-}$), *Jak2*$^{V617F/+}$ *Trp53*$^{R172H/+}$ (J^{VF}P$^{R172H/+}$), and *Jak2*$^{V617F/+}$ *Trp53*$^{R172H/-}$ (J^{VF}P$^{R172H/-}$) mice into recipient mice. Recipient mice transplanted with J^{VF}, J^{VF}P$^{+/-}$, and J^{VF}P$^{R172H/+}$ cells developed an MPN-like phenotype (supplemental Figure 1B) with a median survival of 178 days, 191 days, and 162 days, respectively (Figure 1A). By contrast, the recipients of J^{VF}P$^{-/-}$ and J^{VF}P$^{R172H/-}$ initially developed an MPN phenotype followed by transformation to an acute leukemia phenotype with a median survival of 135 days and 130 days. Survival was significantly shorter in J^{VF}P$^{-/-}$ vs J^{VF}P$^{+/-}$ mice, and in J^{VF}P$^{R172H/-}$ vs J^{VF}P$^{R172H/+}$ mice, and both J^{VF}P$^{-/-}$ and J^{VF}P$^{R172H/-}$ mice had significantly shorted survival than J^{VF} mice (with no significant difference between J^{VF}P$^{-/-}$ and J^{VF}P$^{R172H/-}$mice). Peripheral blood (PB) counts revealed a significant increase in the white blood cell count and spleen weight of J^{VF}P$^{-/-}$ and J^{VF}P$^{R172H/-}$ mice compared with J^{VF} mice, as well as a significant decrease in platelet count and hemoglobin (HGB) in J^{VF}P$^{R172H/-}$ vs J^{VF} mice (Figure 1B). Histopathologic analysis of leukemic mice revealed sheets of immature blast-like cells in the PB, BM, spleen, and liver, which were not observed in J^{VF}, J^{VF}P$^{+/-}$, and J^{VF}P$^{R172H/+}$ mice (Figure 1C). Finally, to confirm that the process of transplantation of hematopoietic stem/progenitor cells (HSPCs) from primary mice did not contribute to the development of the leukemic phenotype observed in J^{VF}P$^{-/-}$ and J^{VF}P$^{R172H/-}$ mice, tamoxifen-induced recombination was conducted in primary mice. J^{VF}P$^{-/-}$ (n = 3) and J^{VF}P$^{R172H/-}$(n = 2) mice developed an MPN phenotype followed by transformation to an acute leukemia, consistent with the earlier observations (supplemental Figure 1C-F). Thus, LT occurred only in the background of *Trp53* biallelic inactivation.

Immunophenotypic analysis revealed CD45$^-$c-Kit$^+$ blast cells, negative for mature myeloid and lymphoid markers (Figure 1D; supplemental Figure 1G), similar to the immunophenotype of human PEL.[21] Furthermore, these blast cells were CD71$^+$Ter119$^-$, and by immunohistochemical stains, blasts were CD45$^-$c-Kit$^+$Gata1$^+$CD71$^+$Ter119$^-$CD41$^-$ blasts (Figure 1E; supplemental Figure 1H), which is consistent with the Bethesda criteria for erythroleukemia in mice.[22]

Functionally, BM cells from J^{VF}P$^{-/-}$ and J^{VF}P$^{R172H/-}$ exhibited increased serial replating capacity, both at the time of LT (Figure 1F) and at the MPN stage (supplemental Figure 1I). The PEL was transplantable to secondary and tertiary recipients, and all recipients rapidly developed lethal PEL (Figure 1G).

The observed latency between the development of an MPN phenotype and a leukemic phenotype suggested the possibility that the process of LT is associated with the acquisition of additional somatic alterations. Using sparse whole-genome sequencing, we identified that the PEL stage (Figure 1H-I), but not its MPN precursor (supplemental Figure 1J), exhibited a complex karyotype (defined as ≥3 karyotypic alterations), with recurrence of acquired events. Mutational analysis identified acquisition of somatic mutations in J^{VF}P$^{-/-}$ and J^{VF}P$^{R172H/-}$ PEL mice without evidence for a clear, additional driver of LT (supplemental Table 1). Although there was no consistent pattern of mutation acquisition observed, the most frequent alterations observed were in *Ptpn11* (largely subclonal). This finding is consistent with prior observations in humans showing that subclonal RAS pathway mutations can occur in *TP53* mutant AML.[23] Thus, *Jak2*^{V617F} and *Trp53* biallelic inactivation results in a highly penetrant form of leukemia that immunophenotypically resembles human PEL and is associated with the development of genomic instability during the process of LT.

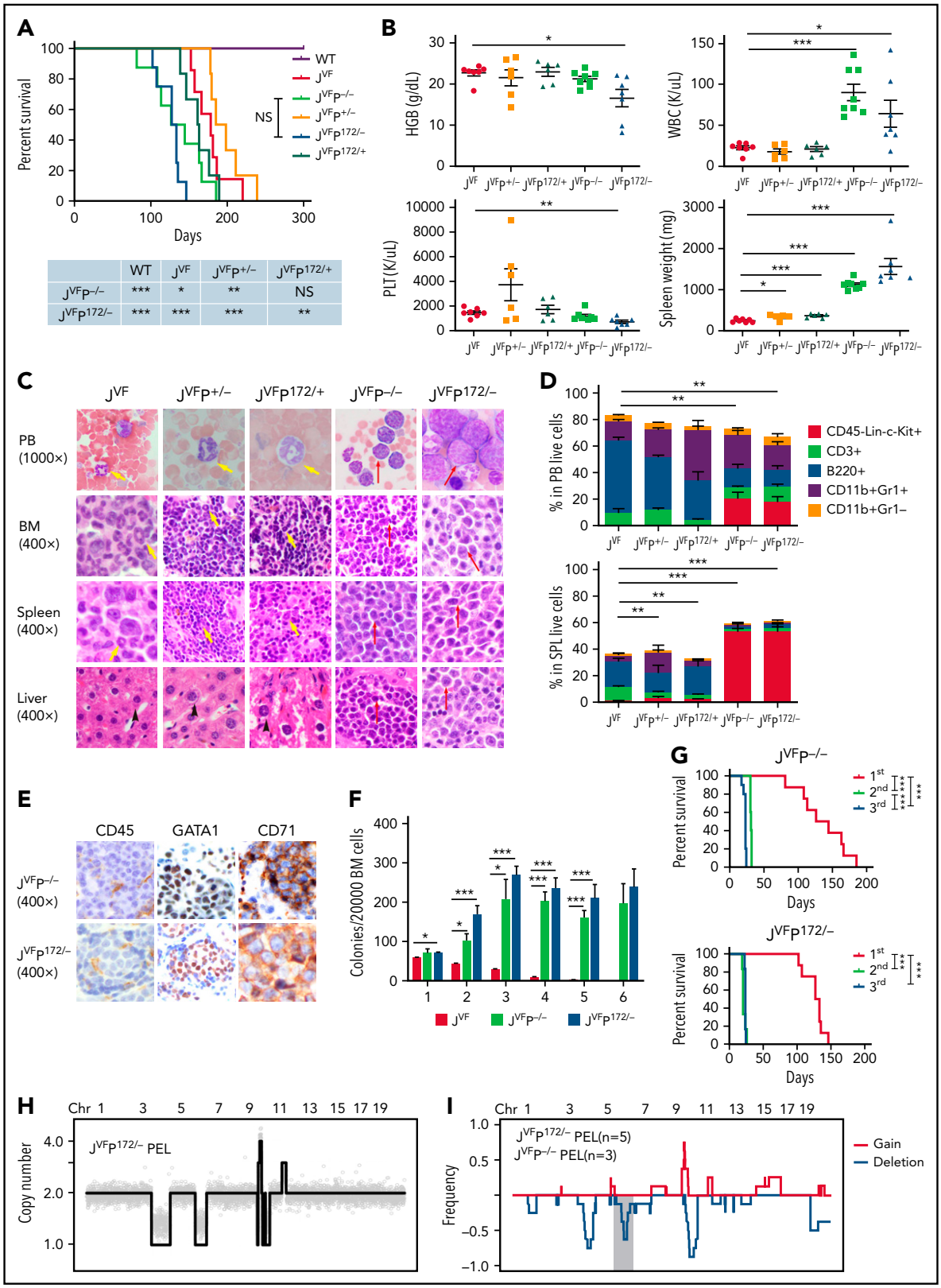

	WT	JVF	JVFP+/−	JVFP172/+
JVFP−/−	***	*	**	NS
JVFP172/−	***	***	***	**

Figure 1. *Jak2*$^{V617F/+}$-*Trp53*$^{-/-}$ and *Jak2*$^{V617F/+}$-*Trp53*$^{R172H/-}$ induce a highly penetrant pure erythroid leukemia. (A) Kaplan-Meier comparative survival analysis of reconstituted mice. Cumulative survival was plotted against days after transplantation. *P* value was determined by the log-rank test. WT control (WT; n = 7); *Jak2*$^{V617F/+}$ (JVF; n = 7); *Jak2*$^{V617F/+}$ *Trp53*$^{+/-}$ (JVFP+/−; n = 6); *Jak2*$^{V617F/+}$ *Trp53*$^{-/-}$ (JVFP−/−; n = 8); *Jak2*$^{V617F/+}$ *Trp53*$^{R172H/+}$ (JVFP172/+; n = 6); *Jak2*$^{V617F/+}$ *Trp53*$^{R172H/-}$ (JVFP172/−; n = 8). JVFP−/− vs JVF, *P* = .0445; JVFP−/− vs JVFP+/−, *P* = .0037; JVFP172/− vs JVF, *P* = .0001; JVFP172/− vs JVFP172/+, *P* = .0016. (B) Complete blood count analysis of PB samples and spleen (SPL) weight collected from moribund PEL JVFP−/− (n = 8), PEL JVFP172/− (n = 8), JVFP+/− (n = 6), JVFP172/+ (n = 6), and JVF (n = 7) mice. JVFP−/− vs JVF: white blood cell (WBC), *P* < .0001; SPL weight, *P* < .0001. JVFP172/− vs JVF: WBC, *P* = .0275; HGB, *P* = .0172; platelet (PLT), *P* = .0016; SPL weight, *P* < .0001. JVFP+/− vs JVF: SPL weight, *P* = .0244. JVFP172/+ vs JVF: SPL weight, *P* = .0005. (C) Wright-Giemsa smear of PB, histopathologic hematoxylin and eosin (H&E) sections of

Megakaryocyte-erythroid progenitor compartment contains the leukemia-initiating population

To identify the leukemia-initiating population, we first examined the proportion of HSPCs pre-LT and post-LT by using flow cytometry. At the MPN stage, the megakaryocyte-erythroid progenitors (MEPs) ($Lin^-c\text{-}Kit^+Sca\text{-}1^-CD34^-FcgRII/III^-$) and LSKs ($Lin^-c\text{-}Kit^+Sca\text{-}1^+$) were significantly expanded in the BM of both $J^{VF}P^{-/-}$ and $J^{VF}P^{R172H/-}$ mice, compared with WT, J^{VF}, $J^{VF}P^{+/-}$, and $J^{VF}P^{R172H/+}$ mice (Figure 2A; supplemental Figure 2A; supplemental Figure 2C). In the spleen, the MEPs, but not the LSKs, were significantly expanded in mice with *Trp53* mutations compared with J^{VF}. No significant change in the size of the granulocyte-macrophage progenitor (GMP) compartment was observed in $J^{VF}P^{-/-}$ and $J^{VF}P^{R172H/-}$ mice (supplemental Figure 2B-C). Significant expansion of the MEPs, but not GMPs, was noted at the time of LT in the BM (Figure 2B). Expansion of the MEPs, GMPs, and LSKs was observed at the time of LT in the spleen; however, the proportional expansion of the MEPs was the greatest among these HSPCs. Notably, in contrast to MEPs from J^{VF} mice, MEPs from leukemic mice did not express CD45 (supplemental Figure 2D).

To further assess the biologic differences of $J^{VF}P^{-/-}$ and $J^{VF}P^{R172H/-}$ HSPCs relative to J^{VF} HSPCs at the MPN stage, competitive transplantation of BM cells from $J^{VF}P^{-/-}$ or $J^{VF}P^{R172H/-}$ and J^{VF} into recipients in a 1:1 ratio was performed (supplemental Figure 2E). PB chimerism revealed that the proportion of $J^{VF}P^{-/-}$ or $J^{VF}P^{R172H/-}$ cells was significantly greater than J^{VF} cells (supplemental Figure 2F). Analysis of BM LSK, MEP, and GMP chimerism at 13 weeks post-tamoxifen revealed that the majority of cells in each HSPC compartment were either $J^{VF}P^{-/-}$ or $J^{VF}P^{R172H/-}$ in origin. Importantly, $J^{VF}P^{-/-}$ comprised a significantly greater proportion of MEPs than GMPs (91% vs 82%) or LSKs (91% vs 62%) (Figure 2C), which was also observed in $J^{VF}P^{R172H/-}$. These data indicate that $J^{VF}P^{-/-}$ or $J^{VF}P^{R172H/-}$ significantly enhances the self-renewal and competitive advantage of HSPCs over J^{VF} HSPCs, most significantly in the MEP compartment.

Given the particular competitive advantages in the MEPs resulting from biallelic *Trp53* inactivation, we hypothesized that the leukemia-initiating population resided in this compartment. To test this hypothesis, we transplanted $CD45^-$ MEPs from $J^{VF}P^{-/-}$ or $J^{VF}P^{R172H/-}$ PEL mice into recipients. These cells were able to efficiently induce a PEL phenotype (supplemental Figure 2G). $CD45^+$ MEPs (early-stage untransformed MEPs relative to $CD45^-$ MEPs) were also able to induce the same PEL phenotype but had a longer latency before onset of PEL (supplemental Figure 2H), suggesting that progression through MEP maturation may be required for leukemic progression. Furthermore, MEPs identified by a distinct set of markers ($Lin^-Sca\text{-}1^-c\text{-}kit^+CD150^+CD41^-CD71^-$ cells, referred to as $CD150^+$ MEPs[24]) also caused PEL with the same immunophenotype as primary recipients. We sought to determine if other HSPC compartments from $J^{VF}P^{-/-}$ and $J^{VF}P^{R172H/-}$ mice contained leukemia-initiating populations at the time of the MPN phenotype. Recipient mice transplanted with MEPs, but not GMPs, developed a PEL phenotype, without a preceding MPN phenotype. Mice transplanted with LSKs also developed a PEL phenotype but with a preceding MPN phenotype, and they also had significantly longer median survival than mice transplanted with MEPs (Figure 2D), suggesting that transition through the MEPs was required for disease initiation.

As shown in Figure 1I, progression of MPN to PEL is characterized by the acquisition of copy number alterations (CNAs), presumably through a process of genomic instability and selection. We would therefore predict that these events might be enriched in the HSPCs containing the leukemia-initiating population and its progeny. Notably, we identified that karyotypic/CNAs were observed in the MEPs and not identified in the GMPs from leukemic mice (Figure 2E-F), although *Jak2* and *Trp53* mutations existed in both populations (supplemental Figure 2I). Collectively, these observations indicate that the biologic and genomic events that lead to leukemic transformation are selected for within the MEPs.

Leukemic population transcriptionally approximates the normal erythroid-committed progenitors

To investigate transcriptional networks in the leukemia-initiating context, we performed scRNA-seq of BM $Lin^-c\text{-}Kit^+$ HSPCs from WT, J^{VF}, pre-PEL $J^{VF}P^{-/-}$, and $J^{VF}P^{-/-}$ PEL mice (supplemental Figure 3A). Clustering analysis of 29 029 single-cell profiles resulted in a detailed map, including 17 transcriptionally homogeneous clusters based on their expression patterns (Figure 3A; supplemental Figure 3B). We further confirmed and defined these HSPC subpopulations and leukemic populations according to canonical surface markers, including CD45 (*Ptprc*), CD34 (*Cd34*), CD16 (*Fcgr3*), CD32 (*Fcgr2b*), CD71 (*Tfrc*), and CD41 (*Itga2b*) (Figure 3B; supplemental Figure 3C). A total of 15 distinct HSPC subpopulations and a leukemic population (consisting of 2 subpopulations, leukemia-1 and leukemia-2) were

Figure 1 (continued) BM, SPL, and liver from representative moribund PEL $J^{VF}P^{-/-}$and $J^{VF}P^{172/-}$, $J^{VF}P^{+/-}$, $J^{VF}P^{172/+}$, and J^{VF} mice. Red arrows indicate blasts, yellow arrows indicate neutrophils, and black arrows indicate hepatocytes. Magnification, 1000× for PB and 400× for BM, SPL, and liver. (D) Proportion of PB cells (top) and SPL cells (bottom) of each lineage and $CD45^-Lin^-c\text{-}Kit^+$ determined by flow cytometric analysis for moribund mice. Lineage markers include CD3, B220, CD11b, and Gr1. J^{VF}, n = 7; PEL $J^{VF}P^{-/-}$, n = 8; PEL $J^{VF}P^{172/-}$, n = 8; $J^{VF}P^{+/-}$, n = 6; $J^{VF}P^{172/+}$, n = 6. Proportion of $CD45^-Lin^-c\text{-}Kit^+$ cells in each murine genotype is compared. PB: $J^{VF}P^{-/-}$ vs J^{VF}, $P = .002$; $J^{VF}P^{172/-}$ vs J^{VF}, $P = .0014$. SPL: $J^{VF}P^{-/-}$ vs J^{VF}, $P < .0001$; $J^{VF}P^{172/-}$ vs J^{VF}, $P < .0001$; $J^{VF}P^{+/-}$ vs J^{VF}, $P = .0021$; $J^{VF}P^{172/+}$ vs J^{VF}, $P = .0018$. (E) Immunohistochemistry (IHC) of liver (CD45, GATA1, and CD71) from representative PEL $J^{VF}P^{-/-}$ and PEL $J^{VF}P^{172/-}$ mice. Magnification, 400×. (F) Methylcellulose replating assay comparing replating capability of whole BM cells from J^{VF}(n = 6), PEL $J^{VF}P^{-/-}$ (n = 8), and PEL $J^{VF}P^{172/-}$ (n = 8) mice. (G) Kaplan-Meier analysis of serial transplant of 1×10^6 whole SPL cells from PEL $J^{VF}P^{-/-}$ and PEL $J^{VF}P^{172/-}$ mice. *P* value was determined by using the log-rank test. First transplant ($J^{VF}P^{-/-}$, n = 8; $J^{VF}P^{172/-}$, n = 8); second transplant ($J^{VF}P^{-/-}$, n = 5; $J^{VF}P^{172/-}$, n = 6); third transplant ($J^{VF}P^{-/-}$, n = 10; $J^{VF}P^{172/-}$, n = 6). $J^{VF}P^{-/-}$: first vs second, $P = .0005$; second vs third, $P = .0005$; first vs third, $P < .0001$. $J^{VF}P^{172/-}$: first vs second, $P = .0002$; first vs third, $P = .0003$. (H) Genome-wide copy number profile of a representative PEL arising from primary transplant of BM cells derived from $J^{VF}P^{172/-}$ donor mouse. Copy number values are rounded to the nearest integer. (I) Frequency plot analysis of a cohort of PEL developing in a p53-deficient background setting ($J^{VF}P^{-/-}$, n = 3; $J^{VF}P^{172/-}$, n = 5). Red lines trace gains, blue lines trace deletions, and gray shading denotes recurrent deletions on mouse chromosome 6. Data are represented as mean ± standard error of the mean (SEM) unless otherwise indicated. The unpaired *t* test was used to compare the mean of 2 groups in panels B, D, and F. $*P < .05$, $**P \leq .01$, $***P \leq .001$.

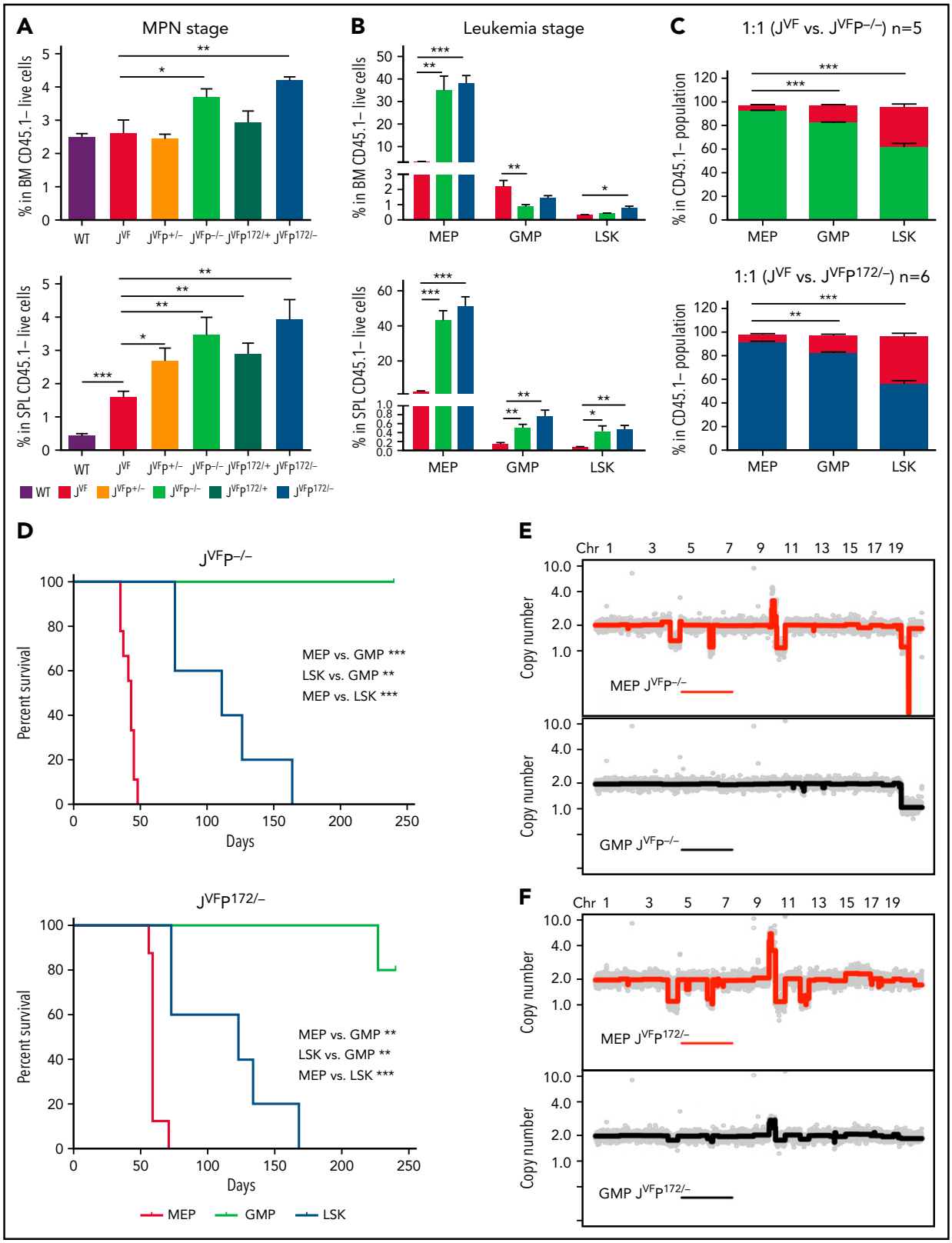

Figure 2. MEP deficient for *Trp53* and expressing *Jak2V617F* are transformed to erythroid leukemia-initiating cells. (A) Percentage of MEPs ($Lin^-c\text{-}Kit^+Sca\text{-}1^-CD34^-FcgRII/III^-$) in the BM (top) and spleen (SPL) (bottom) at MPN stage (8 weeks after transplantation) in each genotype (n = 5 for each group). Data are presented as comparison with J^{VF}. BM: $J^{VF}P^{-/-}$ vs J^{VF}, $P = .0436$; $J^{VF}P^{172/-}$ vs J^{VF}, $P = .004$. SPL: WT vs J^{VF}, $P = .0002$; $J^{VF}P^{+/-}$ vs J^{VF}, $P = .0254$; $J^{VF}P^{-/-}$ vs J^{VF}, $P = .0082$; $J^{VF}P^{172/+}$ vs J^{VF}, $P = .005$; $J^{VF}P^{172/-}$ vs J^{VF}, $P = .0052$. (B) Percentage of MEPs, GMPs ($Lin^-c\text{-}Kit^+Sca\text{-}1^-CD34^+FcgRII/III^+$), and LSKs ($Lin^-c\text{-}Kit^+Sca\text{-}1^+$) in BM (top) and SPL (bottom) from PEL $J^{VF}P^{-/-}$ (n = 8) and $J^{VF}P^{172/-}$ (n = 8) mice or J^{VF} (n = 6) mice as control. Data are presented as comparison with J^{VF}. BM MEP: $J^{VF}P^{-/-}$ vs J^{VF}, $P = .0012$; $J^{VF}P^{172/-}$ vs J^{VF}, $P < .0001$. BM GMP: $J^{VF}P^{-/-}$ vs J^{VF}, $P = .0079$. BM LSK: $J^{VF}P^{172/-}$ vs J^{VF}, $P = .0269$. SPL MEP: $J^{VF}P^{-/-}$ vs J^{VF}, $P < .0001$; $J^{VF}P^{172/-}$ vs J^{VF}, $P < .0001$. SPL GMP: $J^{VF}P^{-/-}$ vs J^{VF}, $P = .005$; $J^{VF}P^{172/-}$ vs J^{VF}, $P = .0033$. SPL LSK: $J^{VF}P^{-/-}$ vs J^{VF}, $P = .0429$; $J^{VF}P^{172/-}$ vs J^{VF}, $P = .0033$. (C) HSPC chimerism (as a

identified (Figure 3C). Compared with J^{VF} mice, the megakaryocyte-erythroid progenitor (MkE-P) and erythroid progenitor (EryP-1 and EryP-2) populations were expanded in pre-PEL $J^{VF}P^{-/-}$ mice (supplemental Figure 3D). To confirm this finding, we used an alternative fluorescence-activated cell sorting (FACS) gating strategy to isolate bipotent MEPs ($Lin^{-}c\text{-}Kit^{+}Sca\text{-}1^{-}CD34^{-}FcgRII/III^{-}CD71^{-}CD41^{-}CD150^{+}CD105^{-}$, referred to as $CD150^{+}CD105^{-}$ MEPs) and erythroid-committed progenitors ($Lin^{-}c\text{-}Kit^{+}Sca\text{-}1^{-}CD34^{-}FcgRII/III^{-}CD71^{+}CD41^{-}$).[25] We observed that $CD150^{+}CD105^{-}$ MEPs and erythroid-committed progenitors were significantly expanded in $J^{VF}P^{-/-}$ and $J^{VF}P^{R172H/-}$ mice at the MPN stage compared with WT and J^{VF} mice (supplemental Figure 3E). Correlation analysis in the average gene expression profile (Figure 3D; supplemental Figure 3F) showed that the leukemia population is most similar to erythroid progenitors and erythroblasts. In addition, analysis of genes upregulated in leukemia-1 and leukemia-2 cells exhibited a significant enrichment in gene sets found in erythroid progenitors (Figure 3E). These data suggest that the leukemia cells evolved from the erythroid lineage.

Given the results indicating that CNAs were found largely in MEPs derived from mice with PEL and the fact that such events were generally large in size, we reasoned that copy-number inference from scRNA-seq data would provide further insights into the specific subpopulations within the MEP compartment associated with LT. Indeed, inference of genome copy number revealed the presence of the previously described CNAs (Figure 2E). Strikingly, these CNAs occurred exclusively in leukemia cells (Figure 3F; supplemental Figure 3G) and not in other populations. Collectively, these data indicate that the leukemic population is a distinct population within the FACS-defined MEP compartment and appears to be most closely transcriptionally related to the normal erythroid progenitor and erythroblast populations. These findings suggest that *Jak2* mutation and *Trp53* deficiency result in transcriptional reprogramming and acquired copy number events that occur in restricted erythroid-committed progenitors.

Leukemia-initiating population resides in the MEP compartment and results in aberrant activation of the bone morphogenetic protein pathway

As described earlier, we observed that both transplanted LSKs and MEPs from $J^{VF}P^{-/-}$ and $J^{VF}P^{R172H/-}$ MPNs give rise to PEL. This raises the question as to whether the leukemia-initiating population resides solely in the MEPs or also in the LSKs. To address this question, we performed RNA-seq on sorted MEPs and LSKs at both the MPN stage and the PEL stage. Three distinct clusters were segregated by principal component analysis (PCA) of these samples: MEPs from PEL, MEPs from non-PEL, and LSKs (Figure 4A). Importantly, in the LSKs of $J^{VF}P^{-/-}$ and $J^{VF}P^{R172H/-}$, no significant differentially expressed genes associated with erythroid differentiation were upregulated (Figure 4B), suggesting that the expansion of the MEPs (Figure 2A) is not due to lineage bias in the LSKs. Furthermore, we did not identify significant differences, relative to WT mice, in the transcriptional signature of the LSK populations in J^{VF}, $J^{VF}P^{+/-}$, $J^{VF}P^{R172H/+}$, $J^{VF}P^{-/-}$, and $J^{VF}P^{R172H/-}$ mice (supplemental Figure 4A). By contrast, evaluation of the MEP populations by gene set enrichment analysis showed an enrichment in stem cell–like signatures in $J^{VF}P^{-/-}$ and $J^{VF}P^{R172H/-}$ MEPs at the MPN stage (Figure 4C). To biologically assess for the presence of stem cell–like features in the MEPs of MPN-stage $J^{VF}P^{-/-}$ and $J^{VF}P^{R172H/-}$ mice, we sorted BM MEPs from $J^{VF}P^{-/-}$, $J^{VF}P^{R172H/-}$, and J^{VF} and assessed for self-renewal capacity by serial replating in methylcellulose medium. Importantly, $J^{VF}P^{-/-}$ and $J^{VF}P^{R172H/-}$ exhibited a significantly increased replating capacity relative to J^{VF} (Figure 4D), thus providing biological validation of the gene set enrichment analysis findings.

To understand the transcriptional programs that distinguish $J^{VF}P^{-/-}$ and $J^{VF}P^{R172H/-}$ erythroleukemic blasts from non-PEL MEPs, we performed RNA-seq and differentially expressed gene analysis (supplemental Figure 4B). Because $J^{VF}P^{-/-}$ and $J^{VF}P^{R172H/-}$ result in an identical phenotype and similar transcriptional programs (supplemental Figure 4C), and to explore the common mechanism by which $Trp53^{-/-}$ and $Trp53^{R172H/-}$ induce $Jak2^{V617F/+}$ MEP transformation, we surveyed pathways associated with the 435 genes upregulated in both $J^{VF}P^{-/-}$ and $J^{VF}P^{R172H/-}$ PEL MEPs. We identified enrichment of the transforming growth factor β/bone morphogenetic protein (BMP) pathway, which was uniquely consistent across 3 data sets among upregulated pathways identified (Figure 4E-G). This pathway is linked to stem cell self-renewal and proliferation.[26,27] Thus, both $J^{VF}P^{-/-}$ and $J^{VF}P^{R172H/-}$ PEL converge on upregulation of the BMP pathway.

Activation of the BMP protein 2/SMAD pathway results in aberrant self-renewal of erythroleukemic blasts

We identified that *Bmp2*, *Bmp4*, *Smad1*, *Smad9*, and *Id1* (a transcriptional target of the BMP/SMAD pathway) were upregulated in $J^{VF}P^{-/-}$ and $J^{VF}P^{R172H/-}$ PEL MEPs relative to WT and J^{VF} (supplemental Figure 5A); this was confirmed via quantitative reverse transcription polymerase chain reaction, western blot, and/or immunohistochemistry (Figure 5A-B; supplemental Figure 5B-C). Furthermore, phosphorylated-SMAD1/5/9 levels (the main SMAD complex through which BMP2 and BMP4 signal) were significantly higher in PEL MEPs compared with J^{VF} (Figure 5C; supplemental Figure 5D) but not in GMPs from PEL (supplemental Figure 5E- F), thus confirming the specific activation of BMP/SMAD pathway in PEL MEPs.

Previous data have shown that BMP2 expression is not enriched in the erythroid lineage in either the human or murine context (https://servers.binf.ku.dk/bloodspot/). This led us to hypothesize

Figure 2 (continued) percentage) in BM of recipient mice transplanted 1:1 with $J^{VF}P^{-/-}$ (n = 5) or $J^{VF}P^{172/-}$ (n = 6) and J^{VF} BM. $J^{VF}P^{-/-}$: MEPs vs GMPs, $P = .0008$; MEPs vs LSKs, $P = .0001$. $J^{VF}P^{172/-}$: MEPs vs GMPs, $P = .0018$; MEPs vs LSKs, $P < .0001$. (D) Kaplan-Meier comparative survival analysis of recipients that were transplanted with LSKs, MEPs, and GMPs from the MPN stage of $J^{VF}P^{-/-}$ (LSKs, n = 5; MEPs, n = 9; GMPs n = 5) or $J^{VF}P^{172/-}$ (LSKs, n = 5; MEPs, n = 8; GMPs, n = 5) mice. *P* value was determined by using the log-rank test. $J^{VF}P^{-/-}$: MEPs vs GMPs, $P = .0007$; LSKs vs GMPs, $P = .0017$; MEPs vs LSKs, $P = .0007$. $J^{VF}P^{172/-}$: MEPs vs GMPs, $P = .0006$; LSKs vs GMPs, $P = .0017$; MEPs vs LSKs, $P = .0006$. (E) Genome-wide copy number profiles of flow cytometry–sorted $J^{VF}P^{-/-}$ MEP (top panel) and GMP (bottom panel) populations after BM transplant and leukemic transformation (n = 4). (F) Genome-wide copy number profiles of flow cytometry–sorted $J^{VF}P^{172/-}$ MEP (top panel) and GMP (bottom panel) populations after BM transplant and leukemic transformation (n = 6). Data are represented as mean ± standard error of the mean (SEM) unless otherwise indicated. The unpaired *t* test was used to compare the mean of 2 groups in panels A, B, and C. $^{*}P < .05$, $^{**}P \leq .01$, $^{***}P \leq .001$.

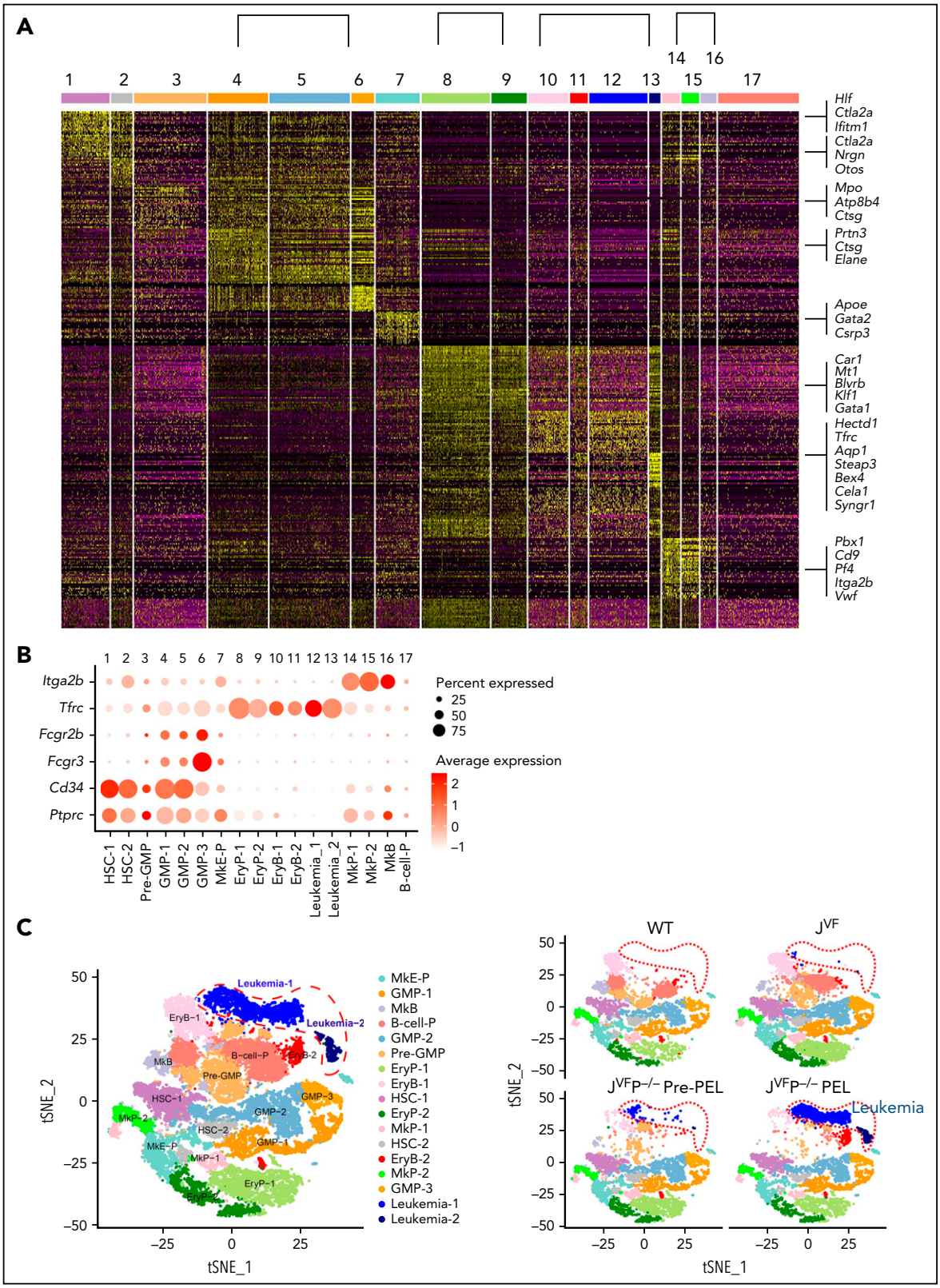

Figure 3. Dynamic changes in *Jak2*$^{V617F/+}$ *Trp53*$^{-/-}$ HSPCs occur during leukemogenesis. (A) Heat map of top representative genes (top 30 genes) for each cluster from single-cell expression profiles. Gene expression profiles of selected marker genes were used to assign cell classification. Columns represent individual cells; rows represent genes. (B) Average expression levels of conventional surface marker genes *Ptprc* (CD45), *Cd34* (CD34), *Fcgr3* (CD16), *Fcgr2b* (CD32), *Tfrc* (CD71), and *Itga2b* (CD41) for single cells in each cluster. Cell clusters were labeled and colored by cell type names: 1, hematopoietic stem cells-1 (HSC-1); 2, HSC-2; 3, Pre-GMP; 4, GMP-1; 5, GMP-2; 6, GMP-3; 7, megakaryocyte-erythroid progenitor (MkE-P); 8, EryP-1; 9, EryP-2; 10, erythroid blast-1 (EryB-1); 11, EryB-2; 12, leukemia-1; 13, leukemia-2; 14, megakaryocyte progenitor-1 (MkP-1); 15, MkP-2; 16, megakaryocyte blast (MkB); and 17, B-cell progenitor (B-cell-P). Dot plot displays average gene expression of surface marker genes for identification of a cluster cell type. The color key from white to red indicates low to high average gene expression level, respectively. The dot

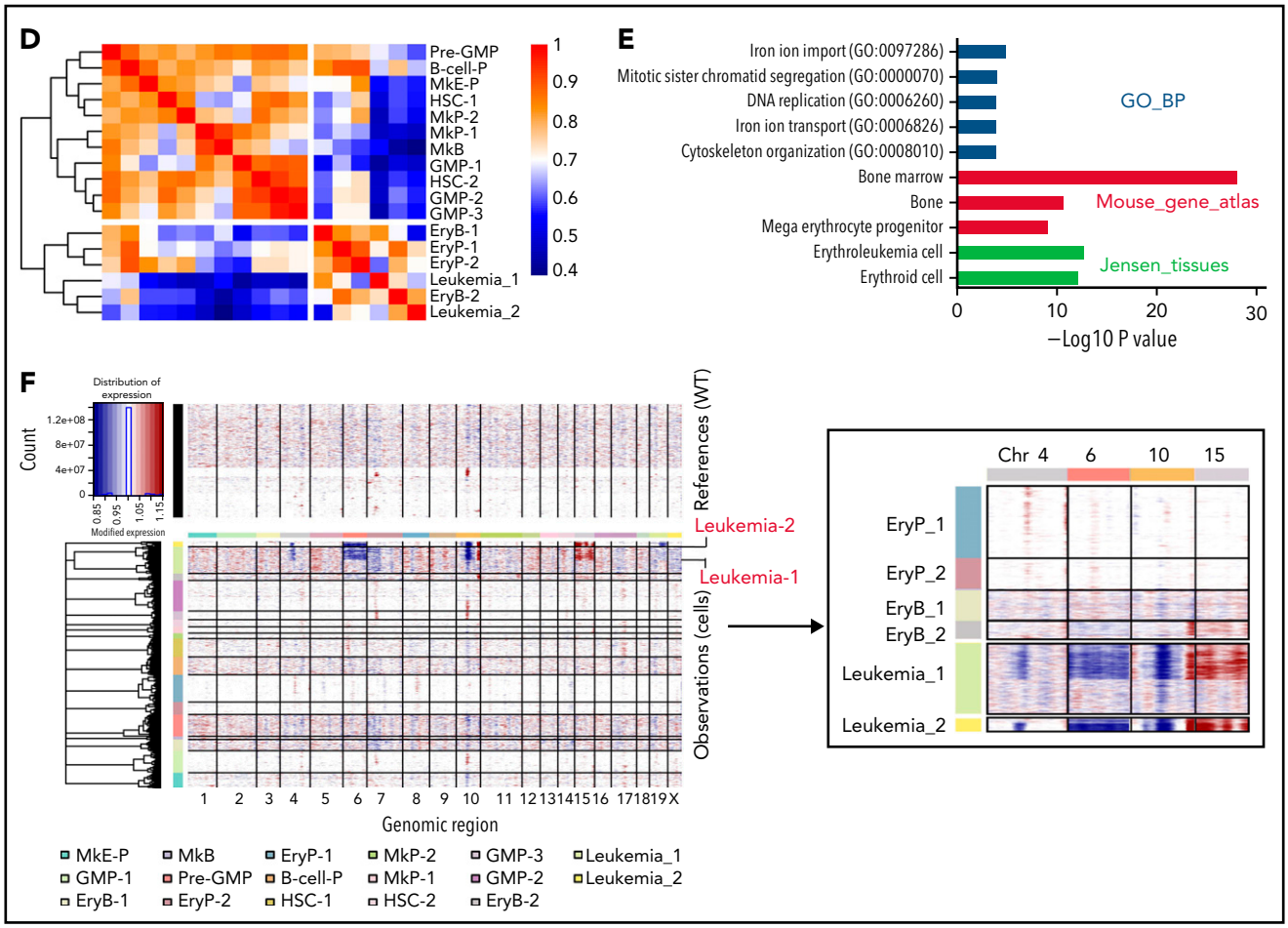

Figure 3 (continued) size indicates percentage of cells expressing a certain marker. (C) Unsupervised graph-based clustering of scRNA-seq data set projected onto a t-distributed stochastic neighbor embedding (t-SNE) plot displaying distinct clusters. A total of 29 029 cells were clustered in the left panel. Each point represents an individual cell. Cell clusters were labeled and colored according to cell type (HSPC subpopulations and leukemic population). In the right panel, t-SNE plot displays subpopulations of HSPCs and leukemic population in a WT, J^{VF}, a pre-PEL $J^{VF}P^{-/-}$, and a PEL $J^{VF}P^{-/-}$ mouse. (D) Heat map of hierarchical clustering of Pearson correlation coefficients between clusters. All coefficients based on the average normalized scRNA-seq data in each cluster. (E) Enrichment analysis of Gene Ontology (GO) and pathways associated with upregulated genes in leukemia cells relative to erythroid progenitors and blasts. (F) Inferred CNA profiles from scRNA-seq data. Chromosomal gains (red) and deletion (blue) are inferred by averaging expression over 100-gene stretches on the respective chromosomes (columns) across the single cells (rows). Top: cells from a WT mouse as reference cells not expected to contain CNVs. Bottom: cells tested for CNAs relative to the reference cells. Zoom in of CNA profiles for leukemia, EryP, and EryB groups on chromosome 4, 6, 10, and 15 (right).

that the observed aberrant expression of BMP2 we observed in PEL MEPs contributed to the process of leukemogenesis. To investigate this possibility, we isolated erythroleukemic blasts ($Lin^-CD45^-c\text{-}Kit^+$ cells) from PEL $J^{VF}P^{-/-}$ and $J^{VF}P^{R172H/-}$ mice and transduced them with viral vectors expressing a short hairpin RNA (shRNA)-targeting *Bmp2* or a control, both with green fluorescent protein (GFP). *Bmp2* knockdown significantly decreased colony formation capacity of erythroleukemic blasts (Figure 5D); upon replating, *Bmp2* knockdown resulted in reduced colony formation at each replating relative to control and almost complete loss of colony formation by the fourth replating for MPN $J^{VF}P^{-/-}$ and $J^{VF}P^{R172H/-}$ MEPs (Figure 5E). Overexpression of *Bmp2* in $c\text{-}Kit^+$ WT BM cells resulted in significantly increased colony formation and increased replating capacity vs controls (Figure 5F). By contrast, *Bmp4* knockdown did not decrease colony formation capacity of erythroleukemic blasts (supplemental Figure 5G-H).

We next investigated the role of *Bmp2* in erythroleukemic blast maintenance in vivo. We transduced erythroleukemic blasts with control shRNA or *Bmp2*-shRNA and injected 5000 GFP^+ transduced erythroleukemic blasts with $CD45.1^+$ WT support BM cells into recipient mice. Recipient mice injected with *Bmp2*-shRNA erythroleukemic blasts showed evidence of restoration of normal hematopoiesis, as evidenced by significant reductions in leukocytosis, significant increases in HGB, and an increase in platelet count (Figure 5G; supplemental Figure 5I). Furthermore, mice that received *Bmp2*-shRNA erythroleukemic blasts exhibited a significant reduction in the representation of GFP^+ transduced erythroleukemic blasts in the PB (Figure 5H; supplemental Figure 5J) and a concomitant increase in the proportion of CD45.1 WT cells in the PB (supplemental Figure 5K), indicating that *Bmp2* silencing abrogated the fitness advantage of erythroleukemic blasts. Finally, compared with mice injected with erythroleukemic blasts with control shRNA, mice injected with *Bmp2*-shRNA erythroleukemic blasts had significantly longer survival (Figure 5I; supplemental Figure 5L).

To determine if the upregulation of the BMP protein 2 (BMP2)/SMAD pathway also occurs in human post-MPN AML, we

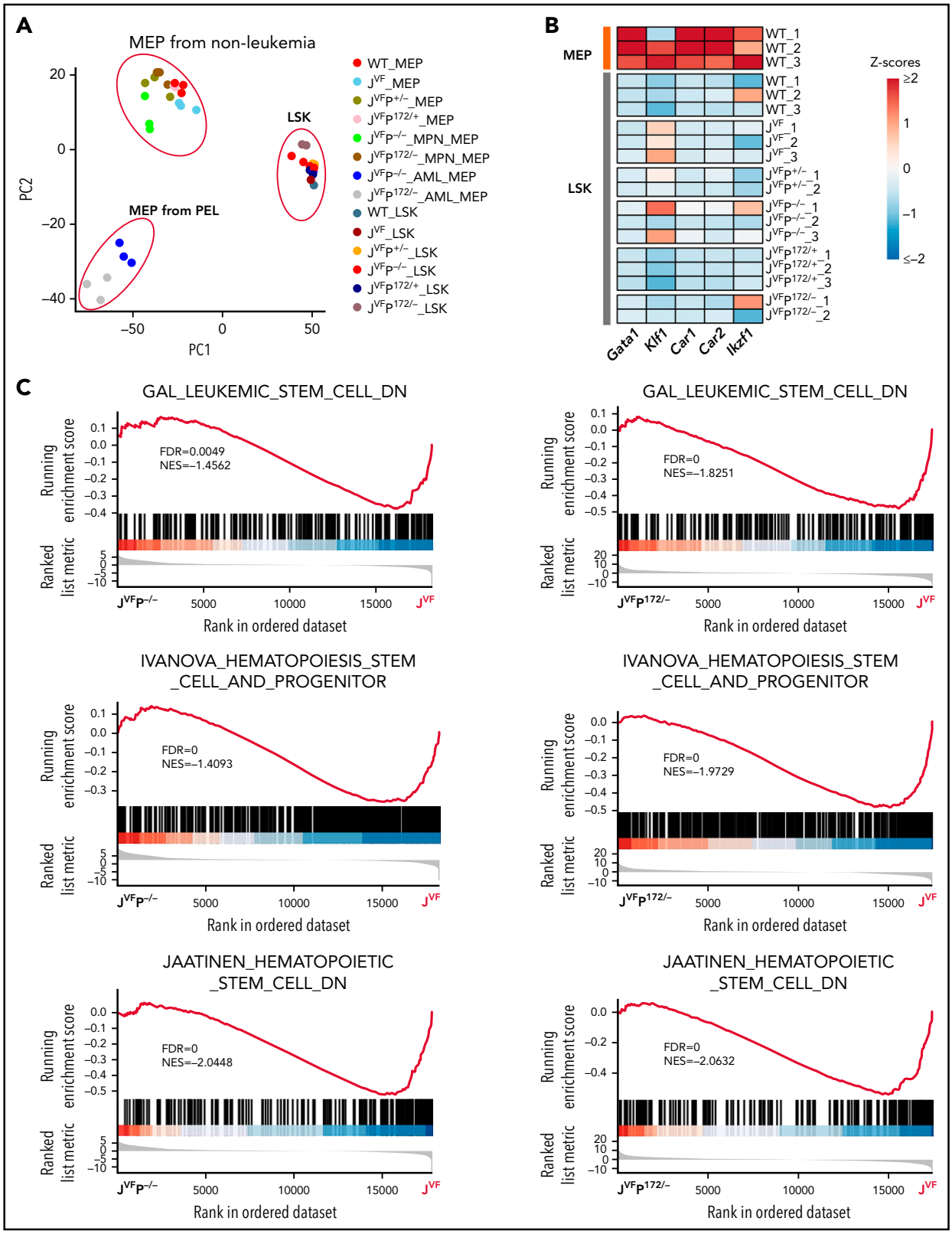

Figure 4. *Jak2*$^{V617F/+}$ *Trp53*$^{-rp}$ and *Jak2*$^{V617F/+}$ *Trp53*$^{R172H/-}$ MEPs are characterized by aberrant gene expression. (A) Principal component analysis (PCA) based on bulk RNA-seq data from flow cytometry–sorted samples. The top 2 components (PC1 and PC2) of the PCA results were used for plot in the plane. (B) Heat map showing representative MEP-priming transcription factor (TFs) expression in WT MEPs and LSKs from WT, J^{VF}, $J^{VF}P^{+/-}$, $J^{VF}P^{-/-}$, $J^{VF}P^{172/+}$, and $J^{VF}P^{172/-}$. (C) Gene set enrichment analysis (GSEA) for comparing gene expression of $J^{VF}P^{-/-}$ and $J^{VF}P^{172/-}$ MPN MEPs vs previously described signatures related to leukemia stem cells or hematopoietic stem cells. (D) Methylcellulose replating assay showing the enhanced replating capability of $J^{VF}P^{-/-}$ and $J^{VF}P^{172/-}$ MPN stage MEPs, relative to J^{VF} MEPs (n = 4 for each genotype). A total of 5000 MEPs were plated per well in the first platting, and 5000 cells from each prior platting were used for subsequent replating. Data are represented as mean ± standard error of the mean (SEM). The unpaired *t* test was used to compare the mean of 2 groups. (E) Bar graphs showing the top

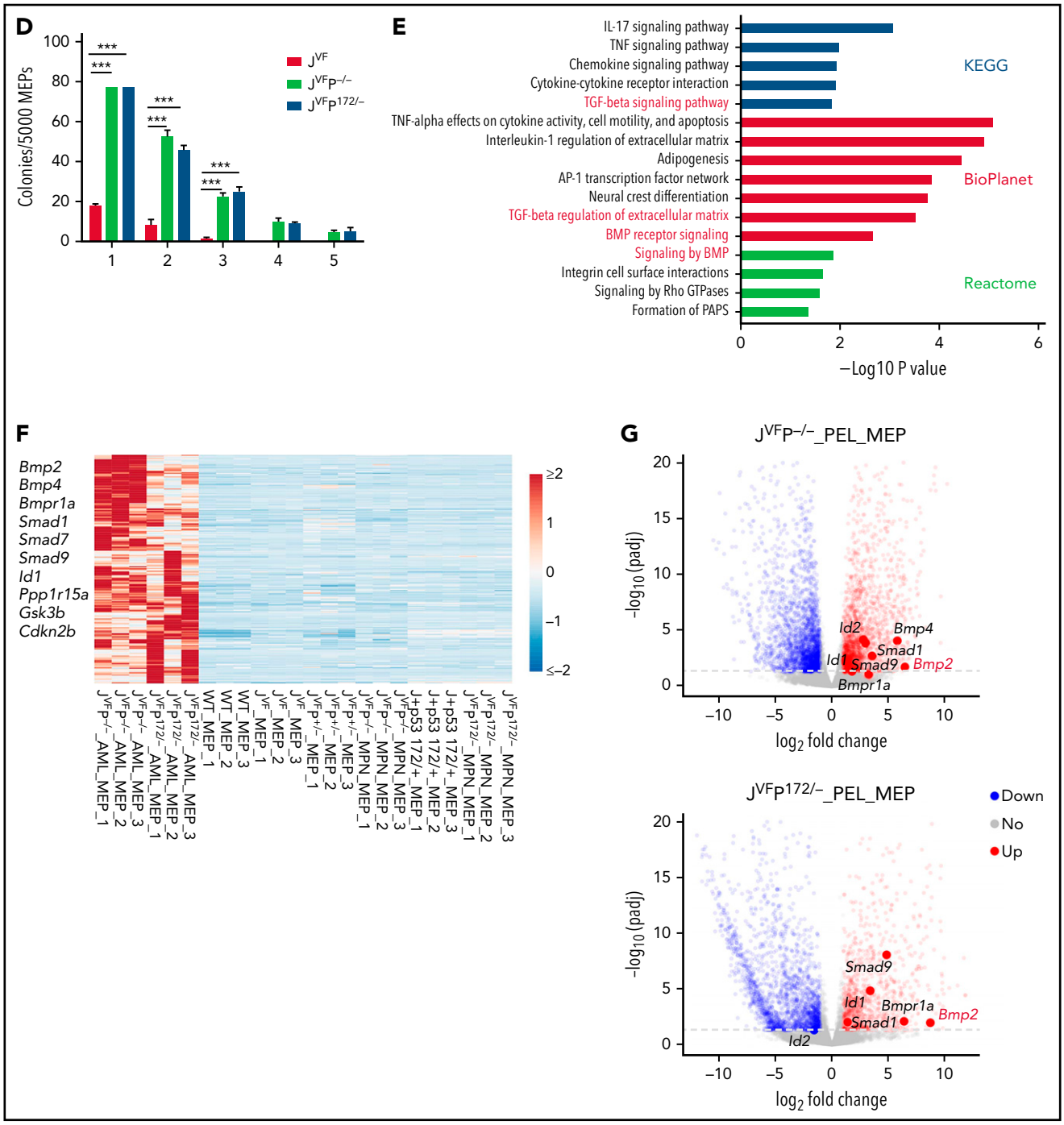

Figure 4 (continued) pathways enriched in $J^{VF}P^{-/-}$ and $J^{VF}P^{172/-}$ PEL MEPs. (F) Heat map of upregulated genes common to $J^{VF}P^{-/-}$ and $J^{VF}P^{172/-}$ PEL MEPs compared with respective controls. (G) Volcano plot from RNA-seq data comparing $J^{VF}P^{-/-}$ and $J^{VF}P^{172/-}$ PEL MEPs vs controls highlighting BMP pathway–related gene expression. *$P \leq .05$, **$P \leq .01$, ***$P \leq .001$.

examined the transcriptional profiles of human post-MPN AML patient samples (either M6/7 or non-M6/7 AML) and identified significant enrichment of BMP2/SMAD pathway expression in post-MPN AML cases relative to cases of polycythemia vera (Figure 5J; supplemental Figure 5M-N). Thus, consistent with our observations in our murine model, the BMP2/SMAD pathway is upregulated in post-MPN AML.

DNA damage response inhibitors show therapeutic efficacy in *Jak2*$^{V617F/+}$ *Trp53*$^{-/-}$ PEL

Prior observations in patients with polycythemia vera have shown that *JAK2*^{V617F} increases replication stress, causing stalling of the replication fork that can be converted to double-strand breaks (DSBs) and impaired intra-S checkpoint in erythroblasts.[28] Moreover, inactivation of p53 results in more DSBs and

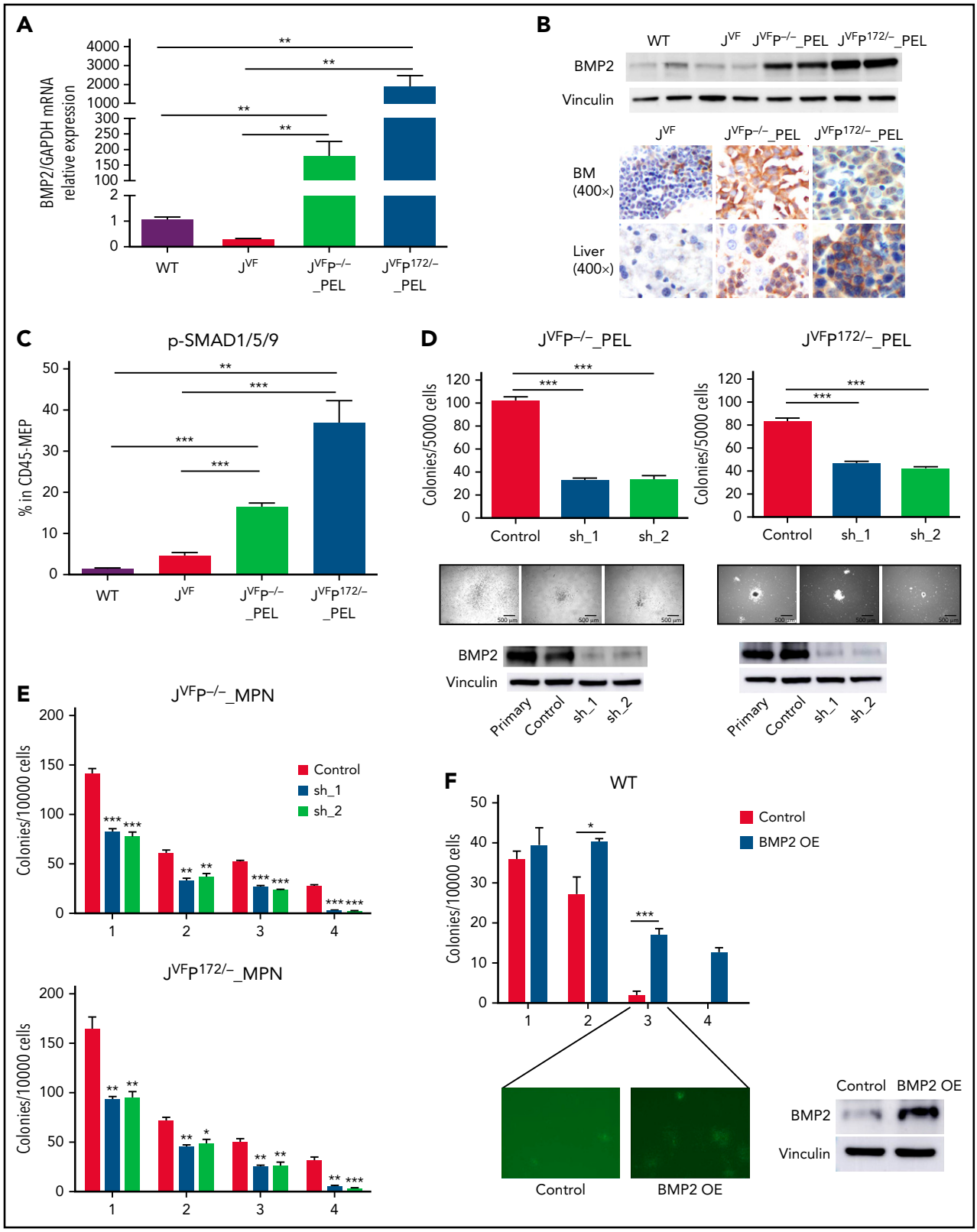

Figure 5. BMP2/SMAD pathway is upregulated in erythroleukemic blasts and contributes to proliferation and self-renewal. (A) Quantitative reverse transcription polymerase chain reaction for *Bmp2* in MEPs from WT, J^{VF}, PEL $J^{VF}P^{-/-}$, and PEL $J^{VF}P^{172/-}$ mice (n = 5-6 mice per genotype). $J^{VF}P^{-/-}$ vs WT, $P = .0064$; $J^{VF}P^{-/-}$ vs J^{VF}, $P = .0062$; $J^{VF}P^{172/-}$ vs WT, $P = .007$; $J^{VF}P^{172/-}$ vs J^{VF}, $P = .007$. (B) Western blot (top) for BMP2 in c-kit$^+$ spleen cells (side-by side duplicates for each murine genotype are presented) and immunohistochemistry (IHC) (bottom) for BMP2 in BM and liver. Magnification, 400×. (C) The fraction of pSMAD1/5/9–positive cells within CD45-MEPs measured by flow cytometry in WT (n = 4), J^{VF} (n = 11), PEL $J^{VF}P^{-/-}$ (n = 12), and PEL $J^{VF}P^{172/-}$ mice (n = 10). $J^{VF}P^{-/-}$ vs J^{VF}, $P < .0001$; $J^{VF}P^{172/-}$ vs J^{VF}, $P < .0001$. (D) Top: total number of colony-forming units (CFUs) generated by $J^{VF}P^{-/-}$ and $J^{VF}P^{172/-}$ erythroleukemic blasts ($Lin^-CD45^-c\text{-}Kit^+$ spleen cells) containing sh. Control (Control), sh.*Bmp2*_1 (sh_1), and sh. *Bmp2*_2 (sh_2) (n = 4 for each group). $J^{VF}P^{-/-}$: sh_1 vs Control, $P < .0001$; sh_2 vs Control, $P < .0001$. $J^{VF}P^{172/-}$: sh_1

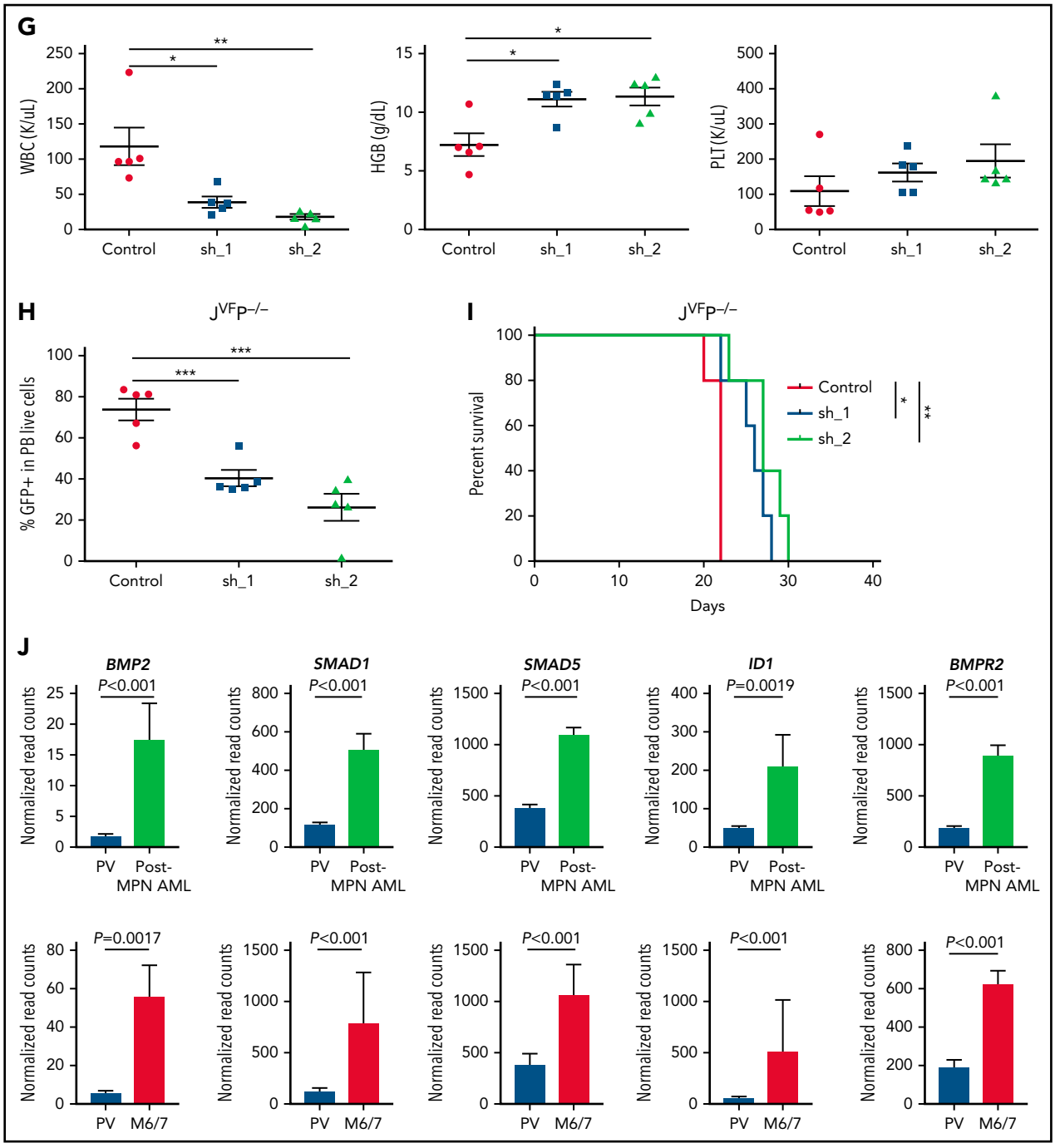

Figure 5 (continued) vs Control, $P < .0001$; sh_2 vs Control $P < .0001$. Middle: representative colonies from each group (magnification, 25×). Bottom: western blot for BMP2 in erythroleukemic blasts with and without *Bmp2* knock down. (E) Methylcellulose replating assay for MPN $J^{VF}P^{-/-}$ and $J^{VF}P^{172/-}$ c-Kit$^+$ BM cells containing sh. Control (Control), sh. *Bmp2*_1 (sh_1), and sh. *Bmp2*_2 (sh_2) (n = 4 for each group). For the first platting, 10 000 GFP$^+$c-Kit$^+$ cells were plated per well. For the second platting and beyond, cells from the prior platting were used for replating (10 000 cells per well). (F) Top: Methylcellulose replating assay for *Bmp2*-overexpressed (OE) in WT BM c-Kit$^+$ cells (n = 4 for each group). For the first platting, 10 000 GFP$^+$c-Kit$^+$ cells were plated per well. For the second platting and beyond, cells from the prior platting were used for replating (10 000 cells per well). Second platting, $P = .029$; third platting, $P = .0004$. Bottom left: Representative CFUs in third round of replating (magnification, 25×). Bottom right: western blot for BMP2 in WT c-Kit$^+$ cells with and without *Bmp2* overexpression. (G) PB counts of recipients transplanted with $J^{VF}P^{-/-}$ erythroleukemic blasts transduced with sh. Control (Control), sh. *Bmp2*_1 (sh_1), and sh. *Bmp2*_2 (sh_2) three weeks after transplantation. N = 4 to 5 mice per arm. White blood cell (WBC): sh_1 vs Control, $P = .0214$; sh_2 vs Control, $P = .0059$. HGB: sh_1 vs Control, $P = .0101$; sh_2 vs Control, $P = .0105$. (H) Percentage of GFP$^+$ cells of PB in recipients transplanted with $J^{VF}P^{-/-}$ erythroleukemic blasts transduced with sh. Control (Control), sh. *Bmp2*_1 (sh_1), and sh. *Bmp2*_2 (sh_2) three weeks after transplantation. N = 4 to 5 mice per arm. sh_1 vs Control, $P = .001$; sh_2 vs Control, $P = .0005$. (I) Kaplan-Meier survival analysis of recipients transplanted with $J^{VF}P^{-/-}$ erythroleukemic blasts transduced with sh. Control (Control), sh. *Bmp2*_1 (sh_1), and sh. *Bmp2*_2 (sh_2). *P* value was determined by the log-rank test. N = 4 to 5 mice per arm. sh_1 vs Control, $P = .0145$; sh_2 vs Control, $P = .0035$. (J) Histogram representation of *BMP2*, *SMAD1*, *SMAD5*, *ID1*, and *BMPR2* gene expression in 14 post-MPN AML cases (including 3 post-MPN M6 and M7) and 9 cases of polycythemia vera (PV). The false discovery rate (FDR)-adjusted *P* values were calculated by DESeq2. Data are represented as mean ± standard error of the mean (SEM). The unpaired *t* test was used to compare the mean of 2 groups in panels A, C, D, E, F, G, and H. $^*P < .05$, $^{**}P \leq .01$, $^{***}P \leq .001$.

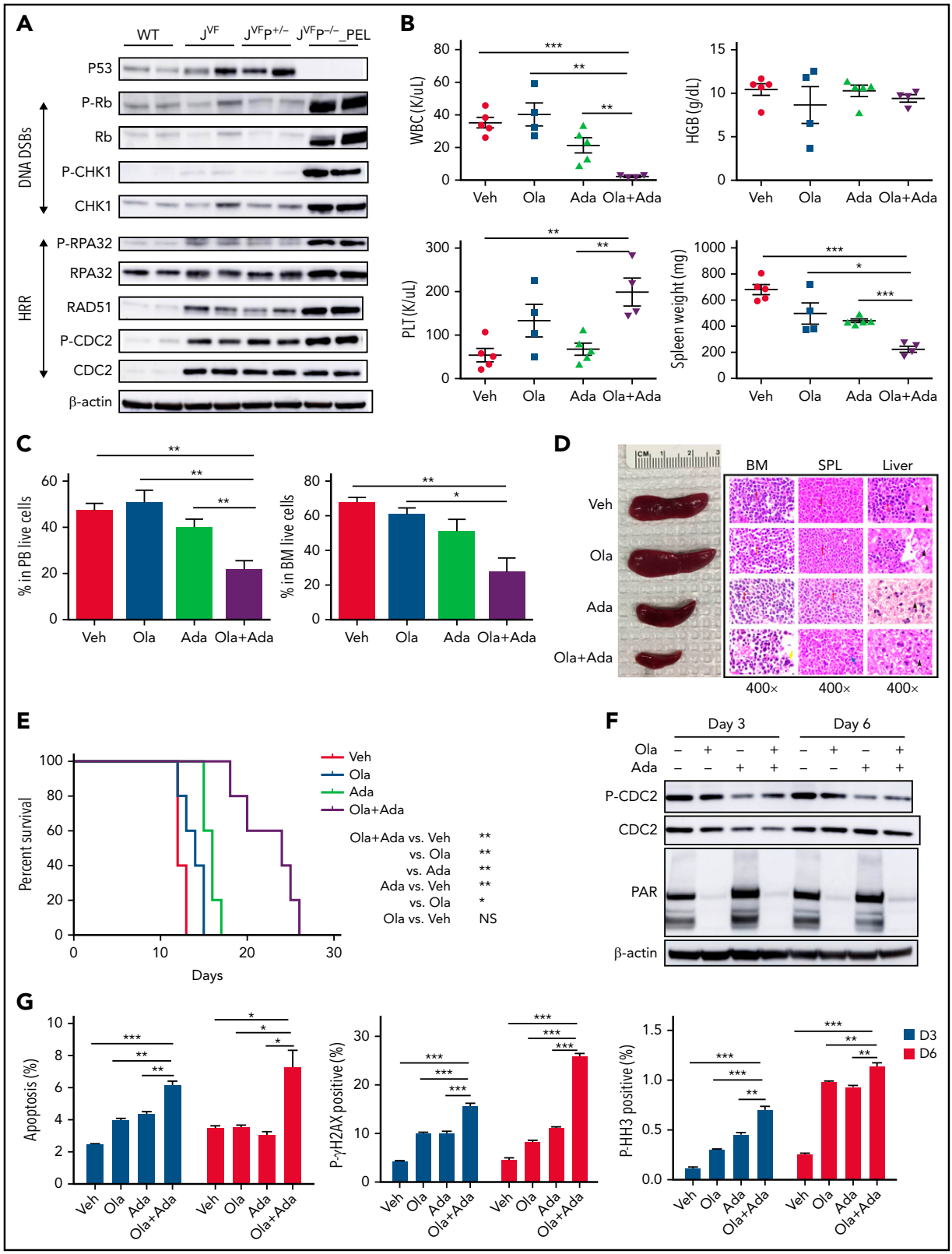

Figure 6. Pharmacodynamic and therapeutic efficacy of PARP and WEE1 inhibition in *Jak2*$^{V617F/+}$ *Trp53*$^{-/-}$ PEL. (A) Western blot analysis of the indicated proteins was performed in duplicate in c-Kit$^+$ spleen cells from WT, J^{VF}, J^{VF}P$^{+/-}$, and PEL J^{VF}P$^{-/-}$ mice. Side-by side duplicates for each murine genotype are presented. (B) PB counts and spleen weights of PEL J^{VF}P$^{-/-}$ from mice treated with vehicle (Veh), olaparib (Ola), adavosertib (Ada), and combination of olaparib and adavosertib (Ola + Ada) after 2 weeks of treatment. N = 4 to 5 mice for each arm. White blood cell (WBC): Ola + Ada vs Veh, $P < .0001$; Ola + Ada vs Ola, $P = .0016$; Ola + Ada vs Ada, $P = .0075$. Platelet (PLT): Ola + Ada vs Veh, $P = .0032$; Ola + Ada vs Ada, $P = .0047$. Spleen weight: Ola + Ada vs Veh, $P < .0001$; Ola + Ada vs Ola, $P = .0171$; Ola + Ada vs Ada, $P < .0001$. (C) Percentage of leukemia cells (CD45$^-$CD3$^-$B220$^-$Gr1$^-$CD11b$^-$c-Kit$^+$) in PB (left) and BM (right) from mice treated with Veh, Ola, Ada, and the Ola + Ada combination after 2 weeks of treatment. N = 4 to 5 mice for each arm. PB: Ola + Ada vs Veh, $P = .0017$; Ola + Ada vs Ola, $P = .0059$; Ola + Ada

exacerbates genomic instability in *JAK2*^{V617F} mutant erythroblasts. Based on these collective observations, we hypothesized that PEL cells have increased activation and dependency on DNA damage response (DDR) pathways for survival. Western blot analysis showed that J^{VF}P$^{-/-}$ PEL c-Kit^{+} spleen cells (compared with WT, J^{VF}, and J^{VF}P$^{+/-}$) had increased expression of phosphorylated RB and CHK1 (associated with DSBs) and phosphorylated RPA32, RAD51, and phosphorylated CDC2 (Y15) (associated with homologous recombination repair) (Figure 6A). Thus, increased activation of DDR was evident in, and largely restricted to, J^{VF}P$^{-/-}$ PEL.

Poly(ADP-ribose) polymerase (PARP) inhibition can result in single-strand breaks that can progress to DSBs if not repaired.[29,30] Inhibition of WEE1 can abrogate G2/M arrest, compromise DNA repair, and allow early mitotic entry of cells harboring unresolved DNA damage, which can result in mitotic catastrophe.[31-33] Prior observations have shown that combined inhibition of WEE1 and PARP results in a synergistic increase in DNA damage and reduction in cellular proliferation in different tumor contexts.[34-37] Given the prior observations regarding the impact of *JAK2*^{V617F} on DNA damage fidelity, the engagement of DDR pathways (as discussed earlier), and the high proliferative rate of erythroleukemic blasts, we investigated the possibility that targeting both PARP and WEE1 could lead to biologically intolerable DNA damage and increased apoptosis in J^{VF}P$^{-/-}$ PEL. We used the WEE1 inhibitor adavosertib and the PARP inhibitor olaparib to treat J^{VF}P$^{-/-}$ leukemic mice. Mice were randomized to treatment with vehicle, olaparib (100 mg/kg daily), adavosertib (60 mg/kg daily), or combination (olaparib 100 mg/kg + adavosertib 60 mg/kg daily) for 2 weeks (pretreatment blood counts at the time of randomization of mice are listed in supplemental Table 2). Compared with vehicle and single agents, combination therapy significantly reduced white blood cell count, leukemic burden in PB and BM, and spleen size (Figure 6B-D). Importantly, the overall survival of mice treated with combination therapy was significantly prolonged compared with controls (Figure 6E). WT mice treated with the combination exhibited a modest decrease in HGB compared with vehicle or single-agent olaparib, but no other hematologic toxicities were observed (supplemental Figure 6A-F).

After 3 days and 6 days of treatment, we evaluated pharmacodynamic markers of WEE1 and PARP inhibitor activity (inhibition of phosphorylation of CDC2, and PAR, respectively) by western blot, which showed inhibition of these pathways in vivo (Figure 6F). Combination therapy significantly increased apoptosis as indicated by cleaved caspase-3 and Annexin V (Figure 6G; supplemental Figure 6G), as well as DNA damage, indicated by phosphorylated RPA32 and phosphorylated γ-H2AX, compared with vehicle and single-agent treatment. The elevated levels of histone H3 (S10) phosphorylation indicated that compared with controls, the combination resulted in a greater proportion of cells in early mitotic entry. These data indicate that combined PARP inhibitor and WEE1 inhibitor treatment promotes DNA damage and induction of apoptosis in J^{VF}P$^{-/-}$ leukemic cells, thus leading to leukemia-specific combination therapeutic efficacy.

Discussion

Acute leukemias characterized by *TP53* mutations with complex karyotypes, including post-MPN AMLs, are associated with lack of therapeutic response to conventional antileukemic therapies and an overall poor prognosis.[38,39] *TP53* alterations reportedly occur in up to 92% of cases of PEL,[40,41] and co-occurring *TP53* mutations and alterations in the 17p locus are frequently observed.[11,40] Collectively, these observations suggest that *TP53* alterations, in distinct genomic contexts such as co-occurring *JAK2* mutations, may result in a convergent propensity toward erythroleukemia characterized by complex cytogenetic alterations. Here, consistent with these clinical observations, we have developed a genomically and biologically accurate model of erythroleukemic transformation of MPNs characterized by CNAs and extensive DNA damage.

Data in solid tumor models have suggested that certain missense mutant *TP53* alleles have gain-of-function (GOF) properties that produce phenotypes distinct from a *TP*53 null state.[42,43] In terms of leukemia, Loizou et al[44] identified a GOF *Trp53*^{R172H} in murine AML. By contrast, in the context of *Jak2*$^{V617F/+}$, we identified no differences in phenotype, karyotype, origin of leukemia, or survival between *Trp53*$^{R172H/-}$ and *Trp53* null PEL. Furthermore, the transcriptional networks of J^{VF}P$^{-/-}$ and J^{VF}P$^{R172H/-}$ PEL share many common molecular signatures. These data provide clear genetic evidence that LT from MPN to acute erythroleukemia requires homozygous inactivation of p53, and that GOF of *TP53* mutations are not responsible for LT in the context of activated JAK2. It provides further evidence for context-specific effects of *TP53* mutations/allelic status, which will need to be investigated in other tumor types using similar approaches.

Our data suggest a distinct lineage bias induced by *Trp53* mutations, including in concert with JAK2 activation in HSPCs evolving to acute leukemia. Lu et al[45] found that *TP53* plays a pivotal

Figure 6 (continued) vs Ada, $P = .0122$. BM: Ola + Ada vs Veh, $P = .002$; Ola + Ada vs Ola, $P = .0133$; Ola + Ada vs Ada, $P = .0723$. (D) Whole spleen specimens and histopathologic hematoxylin and eosin (H&E) sections of BM, spleen, and liver from representative PEL J^{VF}P$^{-/-}$ mice after 2 weeks of treatment with Veh, Ola, Ada, and the Ola + Ada combination. Red arrows indicate blasts, yellow arrow indicates megakaryocytes, blue arrow indicates lymphoid follicle, and black arrow indicates hepatocytes. Magnification, 400×. (E) Kaplan-Meier comparative survival analysis of PEL J^{VF}P$^{-/-}$ mice after 2 weeks of treatment with Veh, Ola, Ada, or the Ola + Ada combination. *P* value was determined by using the log-rank test. N = 5 mice for each arm. Ola + Ada vs Veh, $P = .0039$; Ola + Ada vs Ola, $P = .0027$; Ola + Ada vs Ada, $P = .0019$. (F) Western blot analysis of CDC2 and PAR in c-Kit^{+} spleen cells from J^{VF}P$^{-/-}$ PEL mice treated with Veh, Ola, Ada, or the Ola + Ada combination after 3 and 6 days. (G) PEL J^{VF}P$^{-/-}$ mice were randomized and treated with Veh, Ola, Ada, or the Ola + Ada combination and were euthanized after 3 or 6 days. Whole BM cells were stained with CD45, CD3, B220, Gr1, CD11b, c-Kit, and Annexin V (left), P-γH2AX (middle), or P-HH3 (right) to analyze the apoptosis and DDR in leukemia cells. N = 3 mice for each arm. Annexin V, Day 3: Ola + Ada vs Veh, $P < .0001$; Ola + Ada vs Ola, $P = .0015$; Ola + Ada vs Ada, $P = .0042$; Day 6: Ola + Ada vs Veh, $P = .0232$; Ola + Ada vs Ola, $P = .0241$; Ola + Ada vs Ada, $P = .0167$. P-γH2AX, Day 3: Ola + Ada vs Veh, $P < .0001$; Ola + Ada vs Ola, $P = .0005$; Ola + Ada vs Ada, $P = .0008$; Day 6: Ola + Ada vs Veh, $P < .0001$; Ola + Ada vs Ola, $P < .0001$; Ola + Ada vs Ada, $P < .0001$. P-HH3, Day 3: Ola + Ada vs Veh, $P < .0001$; Ola + Ada vs Ola, $P = .0002$; Ola + Ada vs Ada, $P = .0025$; Day 6: Ola + Ada vs Veh, $P < .0001$; Ola + Ada vs Ola, $P = .009$; Ola + Ada vs Ada, $P = .0041$. Data are represented as mean ± standard error of the mean (SEM). The unpaired *t* test was used to compare the mean of 2 groups in panels B, C, and G. $^{*}P < .05$, $^{**}P \leq .01$, $^{***}P \leq .001$. HRR, homologous recombination repair.

role in erythroid progenitor fate specification. Furthermore, in conditions of stress erythropoiesis, the absence of p53 increases the proliferation of erythroid progenitors and immature precursors.[46] FACS-defined MEPs represent a heterogeneous population, and transformation in our models occurs within this compartment but cannot be further resolved by flow cytometric analysis alone.[47] Our scRNA-seq data suggest that p53 inactivation expands bipotent MkE-P, promotes erythrocyte-committed expansion, and facilitates the transformation of erythroid progenitors in the context of *Jak2* constitutive activation. These data suggest a key regulatory role for p53 in erythroid lineage maturation in the context of certain physiologic stresses, providing a key barrier to transformation that is overcome by concurrent JAK2 activation plus biallelic *Trp53* loss.

We identified that the BMP/SMAD pathway has a key role in the pathogenesis of p53 mutant LT. BMPs have been implicated in the self-renewal and maintenance of HSCs, as well as regulating the expansion of progenitor cells.[48] In adult erythropoiesis, exposure to exogenous BMP2 increases immature erythroid colonies.[49] Moreover, upregulation of the BMP2/4 pathway also plays a role in enhancing self-renewal of megakaryocytic progenitors in pediatric acute megakaryoblastic leukemia with inv(16)(p13.3q24.3).[50] Interestingly, the BMP2/SMAD pathway appears to play a role in DDR.[51] Whether the BMP2/SMAD pathway becomes upregulated in response to the increased DNA damage incurred during leukemic progression remains to be investigated.

In summary, we have developed murine models of *Jak2-Trp53*–altered erythroleukemia characterized by recurrent CNAs and DNA damage that faithfully recapitulate the key features of human erythroleukemia. The process of LT is characterized by upregulation of the BMP/SMAD pathway, which enhances self-renewal and HSPC expansion. Importantly, we identify that the resulting increase in DNA damage can be exploited by exposure to DDR pathway inhibitors, suggesting that combined WEE1/PARP inhibition as a therapeutic approach to treat this high risk, refractory leukemia subtype is urgently warranted in the preclinical to clinical context.

Acknowledgments

This study was supported by a National Institutes of Health, National Cancer Institute (NCI), Cancer Center Support Grant/Core Grant to Memorial Sloan Kettering Cancer Center (P30 CA008748), NCI grants (1K08CA188529-01, R.K.R.; R35 CA197594-01A1, R.L.L.; and P01 CA108671 11, R.L.L. and R.K.R.), the Kattamuri S. Sarma Leukemia Research Fund, and a grant from Cycle for Survival (R.K.R). B.L. is supported by National Natural Science Foundation of China (NSFC) (82070134) and Tianjin Natural Science Funds (19JCQNJC09400), and NSFC 81530008 (Z.X.). H.W. and K.H. are supported by a Tri-Institutional Stem Cell grant (2019-035). T.B. is supported by the William C. and Joyce C. O'Neil Charitable Trust, Memorial Sloan-Kettering Single Cell Sequencing Initiative. C.G.M. and I.I. are supported by the American Lebanese Syrian Associated Charities of St. Jude Children's Research Hospital. C.G.M. is supported by NCI R35 Outstanding Investigator Award CA197695, the Henry Schueler 41&9 Foundation, and a Leukemia and Lymphoma Society Translational Research Program. I.I. is supported by the St. Jude Children's Research Hospital Hematological Malignancies Program Garwood Fellowship. S.W.L. is supported by NCI 1 P50 CA254838-01.

Authorship

Contribution: R.K.R., R.L.L., B.L., W.A., and H.W. conceived the project; B.L., W.A., H.W., T.B., S.M., A.K., W.X., and Y.L. performed and analyzed experiments; R.P.K. and H.W. performed bioinformatics analyses; I.I. and C.G.M. provided patient RNA-seq data; B.L., W.A., H.W., and R.K.R. wrote the original draft; S.F.C., Z.X., A.D., K.H., S.W.L., R.L.L., and R.K.R. reviewed and edited the original draft; and R.L.L. and R.K.R. supervised the project. All authors reviewed and approved the manuscript.

Conflict-of-interest disclosure: R.K.R. has received consulting fees from Constellation, Incyte, Celgene/BMS, Novartis, Promedior, CTI, Jazz Pharmaceuticals, Blueprint, Stemline, Galecto, PharmaEssentia, AbbVie, Sierra Oncology, and Disc Medicines; and research funding from Incyte, Constellation, and Stemline. R.L.L. is on the supervisory board of QIAGEN; is a scientific advisor to Loxo (until February 2019), Imago, C4 Therapeutics, and IsoPlexis; receives research support from and consulted for Celgene and Roche; has consulted for Lilly, Jubilant, Janssen, Astellas, MorphoSys, and Novartis; and has received honoraria from Roche, Lilly, and Amgen for invited lectures and from Celgene and Gilead for grant reviews. C.G.M. has received research funding from AbbVie and Pfizer, speaking fees from Amgen, and advisory board fees from Illumina; and holds stock in Amgen. I.I. received honoraria from Amgen and Mission Bio. K.H. is a founder of Dania Therapeutics; a consultant for Inthera Bioscience AG; and a scientific advisor for MetaboMed Inc. and Hannibal Health Innovation. S.W.L. is a founder and member of the scientific advisory board of Blueprint Medicines, Mirimus, ORIC Pharmaceuticals, and Faeth Therapeutics; and is on the scientific advisory board of Constellation Pharmaceuticals and PMV Pharmaceuticals. The remaining authors declare no competing financial interests.

The current affiliation for K.H. is Institute of Cancer Research, London, United Kingdom.

ORCID profiles: B.L., 0000-0002-8291-9883; A.K., 0000-0001-6191-5966; W.X., 0000-0001-8586-8500; Y.L., 0000-0002-9167-3205; A.D., 0000-0003-2178-8493; C.G.M., 0000-0002-1871-1850; K.H., 0000-0003-1975-6097.

Correspondence: Raajit K. Rampal, Leukemia Service, Department of Medicine, 530 East 74th st, New York, NY 10021; e-mail: rampalr@mskcc.org.

Footnotes

Submitted 21 October 2021; accepted 24 March 2022; prepublished online on *Blood* First Edition 16 April 2022. DOI 10.1182/blood.2021014465.

*B.L., W.A., and H.W. contributed equally to this work as first authors.

The RNA-seq and scRNA-seq data sets are available and deposited in the Gene Expression Omnibus database (accession number GSE180853).

The online version of this article contains a data supplement.

There is a *Blood* Commentary on this article in this issue.

The publication costs of this article were defrayed in part by page charge payment. Therefore, and solely to indicate this fact, this article is hereby marked "advertisement" in accordance with 18 USC section 1734.

REFERENCES

1. James C, Ugo V, Le Couédic JP, et al. A unique clonal JAK2 mutation leading to constitutive signalling causes polycythaemia vera. *Nature*. 2005;434(7037):1144-1148.
2. Levine RL, Wadleigh M, Cools J, et al. Activating mutation in the tyrosine kinase JAK2 in polycythemia vera, essential thrombocythemia, and myeloid metaplasia with myelofibrosis. *Cancer Cell*. 2005;7(4):387-397.
3. Baxter EJ, Scott LM, Campbell PJ, et al; Cancer Genome Project. Acquired mutation of the tyrosine kinase JAK2 in human myeloproliferative disorders. *Lancet*. 2005;365(9464):1054-1061.
4. Kralovics R, Passamonti F, Buser AS, et al. A gain-of-function mutation of JAK2 in myeloproliferative disorders. *N Engl J Med*. 2005;352(17):1779-1790.
5. Mesa RA, Li CY, Ketterling RP, Schroeder GS, Knudson RA, Tefferi A. Leukemic transformation in myelofibrosis with myeloid metaplasia: a single-institution experience with 91 cases. *Blood*. 2005;105(3):973-977.
6. Chihara D, Kantarjian HM, Newberry KJ, et al. Survival outcome of patients with acute myeloid leukemia transformed from myeloproliferative neoplasms. *Blood*. 2016;128(22):1940.
7. Rampal R, Ahn J, Abdel-Wahab O, et al. Genomic and functional analysis of leukemic transformation of myeloproliferative neoplasms. *Proc Natl Acad Sci U S A*. 2014;111(50):E5401-E5410.
8. Grinfeld J, Nangalia J, Baxter EJ, et al. Classification and personalized prognosis in myeloproliferative neoplasms. *N Engl J Med*. 2018;379(15):1416-1430.
9. Courtier F, Carbuccia N, Garnier S, et al. Genomic analysis of myeloproliferative neoplasms in chronic and acute phases. *Haematologica*. 2017;102(1):e11-e14.
10. Harutyunyan A, Klampfl T, Cazzola M, Kralovics R. p53 lesions in leukemic transformation. *N Engl J Med*. 2011;364(5):488-490.
11. Chernak BJ, Sen F, Farnoud N, et al. Atypical presentation of erythroid/megakaryocytic leukemic transformation of a myeloproliferative neoplasm associated with mutation and loss of TP53. *HemaSphere*. 2020;4(4):e411.
12. Lundberg P, Karow A, Nienhold R, et al. Clonal evolution and clinical correlates of somatic mutations in myeloproliferative neoplasms. *Blood*. 2014;123(14):2220-2228.
13. Kubesova B, Pavlova S, Malcikova J, et al. Low-burden TP53 mutations in chronic phase of myeloproliferative neoplasms: association with age, hydroxyurea administration, disease type and JAK2 mutational status. *Leukemia*. 2018;32(2):450-461.
14. Bernard E, Nannya Y, Hasserjian RP, et al. Implications of TP53 allelic state for genome stability, clinical presentation and outcomes in myelodysplastic syndromes [published corrections appear in *Nat Med*. 2021;27(3):562 and 2021;27(5):927]. *Nat Med*. 2020;26(10):1549-1556.
15. Boettcher S, Miller PG, Sharma R, et al. A dominant-negative effect drives selection of *TP53* missense mutations in myeloid malignancies. *Science*. 2019;365(6453):599-604.
16. Mullally A, Lane SW, Ball B, et al. Physiological Jak2V617F expression causes a lethal myeloproliferative neoplasm with differential effects on hematopoietic stem and progenitor cells. *Cancer Cell*. 2010;17(6):584-596.
17. Olive KP, Tuveson DA, Ruhe ZC, et al. Mutant p53 gain of function in two mouse models of Li-Fraumeni syndrome. *Cell*. 2004;119(6):847-860.
18. Marino S, Vooijs M, van Der Gulden H, Jonkers J, Berns A. Induction of medulloblastomas in p53-null mutant mice by somatic inactivation of Rb in the external granular layer cells of the cerebellum. *Genes Dev*. 2000;14(8):994-1004.
19. Abdel-Wahab O, Gao J, Adli M, et al. Deletion of Asxl1 results in myelodysplasia and severe developmental defects in vivo. *J Exp Med*. 2013;210(12):2641-2659.
20. Rampal RK, Pinzon-Ortiz M, Somasundara AVH, et al. Therapeutic efficacy of combined JAK1/2, Pan-PIM, and CDK4/6 inhibition in myeloproliferative neoplasms. *Clin Cancer Res*. 2021;27(12):3456-3468.
21. Arber DA, Orazi A, Hasserjian R, et al. The 2016 revision to the World Health Organization classification of myeloid neoplasms and acute leukemia. *Blood*. 2016;127(20):2391-2405.
22. Kogan SC, Ward JM, Anver MR, et al; Hematopathology subcommittee of the Mouse Models of Human Cancers Consortium. Bethesda proposals for classification of nonlymphoid hematopoietic neoplasms in mice. *Blood*. 2002;100(1):238-245.
23. Welch JS. Patterns of mutations in TP53 mutated AML. *Best Pract Res Clin Haematol*. 2018;31(4):379-383.
24. Rieger MA, Smejkal BM, Schroeder T. Improved prospective identification of megakaryocyte-erythrocyte progenitor cells. *Br J Haematol*. 2009;144(3):448-451.
25. Pronk CJ, Rossi DJ, Månsson R, et al. Elucidation of the phenotypic, functional, and molecular topography of a myeloerythroid progenitor cell hierarchy. *Cell Stem Cell*. 2007;1(4):428-442.
26. Ying QL, Nichols J, Chambers I, Smith A. BMP induction of Id proteins suppresses differentiation and sustains embryonic stem cell self-renewal in collaboration with STAT3. *Cell*. 2003;115(3):281-292.
27. Lengerke C, Schmitt S, Bowman TV, et al. BMP and Wnt specify hematopoietic fate by activation of the Cdx-Hox pathway. *Cell Stem Cell*. 2008;2(1):72-82.
28. Chen E, Ahn JS, Massie CE, et al. JAK2V617F promotes replication fork stalling with disease-restricted impairment of the intra-S checkpoint response. *Proc Natl Acad Sci U S A*. 2014;111(42):15190-15195.
29. Amé JC, Spenlehauer C, de Murcia G. The PARP superfamily. *BioEssays*. 2004;26(8):882-893.
30. Pommier Y, O'Connor MJ, de Bono J. Laying a trap to kill cancer cells: PARP inhibitors and their mechanisms of action. *Sci Transl Med*. 2016;8(362):362ps17.
31. Porter CC, Kim J, Fosmire S, et al. Integrated genomic analyses identify WEE1 as a critical mediator of cell fate and a novel therapeutic target in acute myeloid leukemia. *Leukemia*. 2012;26(6):1266-1276.
32. Guertin AD, Li J, Liu Y, et al. Preclinical evaluation of the WEE1 inhibitor MK-1775 as single-agent anticancer therapy. *Mol Cancer Ther*. 2013;12(8):1442-1452.
33. Ghelli Luserna Di Rorà A, Beeharry N, Imbrogno E, et al. Targeting WEE1 to enhance conventional therapies for acute lymphoblastic leukemia. *J Hematol Oncol*. 2018;11(1):99.
34. Fang Y, McGrail DJ, Sun C, et al. Sequential therapy with PARP and WEE1 inhibitors minimizes toxicity while maintaining efficacy. *Cancer Cell*. 2019;35(6):851-867.e7.
35. Lallo A, Frese KK, Morrow CJ, et al. The combination of the PARP inhibitor olaparib and the WEE1 inhibitor AZD1775 as a new therapeutic option for small cell lung cancer. *Clin Cancer Res*. 2018;24(20):5153-5164.
36. Garcia TB, Snedeker JC, Baturin D, et al. A small-molecule inhibitor of WEE1, AZD1775, synergizes with olaparib by impairing homologous recombination and enhancing DNA damage and apoptosis in acute leukemia. *Mol Cancer Ther*. 2017;16(10):2058-2068.
37. O'Connor MJ. Targeting the DNA damage response in cancer. *Mol Cell*. 2015;60(4):547-560.
38. Rücker FG, Schlenk RF, Bullinger L, et al. TP53 alterations in acute myeloid leukemia with complex karyotype correlate with specific copy number alterations, monosomal karyotype, and dismal outcome. *Blood*. 2012;119(9):2114-2121.
39. Rücker FG, Dolnik A, Blätte TJ, et al. Chromothripsis is linked to *TP53* alteration, cell cycle impairment, and dismal outcome in acute myeloid leukemia with complex karyotype. *Haematologica*. 2018;103(1):e17-e20.
40. Montalban-Bravo G, Benton CB, Wang SA, et al. More than 1 *TP53* abnormality is a dominant characteristic of pure erythroid leukemia. *Blood*. 2017;129(18):2584-2587.
41. Iacobucci I, Wen J, Meggendorfer M, et al. Genomic subtyping and therapeutic targeting of acute erythroleukemia. *Nat Genet*. 2019;51(4):694-704.
42. Weissmueller S, Manchado E, Saborowski M, et al. Mutant p53 drives pancreatic cancer metastasis through cell-autonomous PDGF receptor β signaling. *Cell*. 2014;157(2):382-394.

43. Schulz-Heddergott R, Stark N, Edmunds SJ, et al. Therapeutic ablation of gain-of-function mutant p53 in colorectal cancer inhibits Stat3-mediated tumor growth and invasion. *Cancer Cell*. 2018;34(2):298-314.e7.

44. Loizou E, Banito A, Livshits G, et al. A gain-of-function p53-mutant oncogene promotes cell fate plasticity and myeloid leukemia through the pluripotency factor FOXH1. *Cancer Discov*. 2019;9(7):962-979.

45. Lu YC, Sanada C, Xavier-Ferrucio J, et al. The molecular signature of megakaryocyte-erythroid progenitors reveals a role for the cell cycle in fate specification [published correction appears in *Cell Rep*. 2018;25(11):3229]. *Cell Rep*. 2018;25(8):2083-2093.e4.

46. Le Goff S, Boussaid I, Floquet C, et al. p53 activation during ribosome biogenesis regulates normal erythroid differentiation. *Blood*. 2021;137(1):89-102.

47. Xavier-Ferrucio J, Krause DS. Bipotent megakaryocytic-erythroid progenitors: concepts and controversies. *Stem Cells*. 2018;36(8):1138-1145.

48. Toofan P, Irvine D, Hopcroft L, Copland M, Wheadon H. The role of the bone morphogenetic proteins in leukaemic stem cell persistence. *Biochem Soc Trans*. 2014;42(4):809-815.

49. Maguer-Satta V, Bartholin L, Jeanpierre S, et al. Regulation of human erythropoiesis by activin A, BMP2, and BMP4, members of the TGFbeta family. *Exp Cell Res*. 2003;282(2):110-120.

50. Gruber TA, Larson Gedman A, Zhang J, et al. An Inv(16)(p13.3q24.3)-encoded CBFA2T3-GLIS2 fusion protein defines an aggressive subtype of pediatric acute megakaryoblastic leukemia. *Cancer Cell*. 2012;22(5):683-697.

51. Chau JF, Jia D, Wang Z, et al. A crucial role for bone morphogenetic protein-Smad1 signalling in the DNA damage response. *Nat Commun*. 2012;3(1):836.